Bachelor Thesis

Degree Project in
Geology 15 hp

Igneous rocks of the Ivrea-Verbano Zone, Italian Alps

Francis Long

Stockholm 2024

Department of Geological Sciences
Stockholm University
SE-106 91 Stockholm

Abstract

The Ivrea-Verbano Zone (IVZ) in the Italian alps is approximately 100km northwest of Milan. The IVZ is home to, a large igneous intrusion called the Mafic Complex (MC), metasediments that make up the Kinzigite Formation (KZ), and granitic plutons (Granitoids). The MC is significant because it provides a rare glimpse of the mantle which is otherwise out of reach. This study investigates the mantle source of this body of mafic rocks and the effect its emplacement had on the IVZ. The MC magma was extracted from an 80 km deep mantle source, underwent plagioclase and olivine fractionation, and had a potential rejuvenation event based on both petrological evidence and geochemical signatures. Based on the decoupling of the Large Ion Lithophile elements (LILE) and the High Field Strength elements (HFSE), the MC has a subduction related origin. No correlation was found between the MC and the KZ and Granitoids of the IVZ, however there is probable cause for suggesting that metamorphism of the KZ generated the Granitoids. From this correlation, the Granitoids are suggested to be result from decompression melting associated with the laterally spreading, newly formed Alps in the Permian.

Table of Contents

Introduction

In the Italian alps, an area of petrological significance exists called the Ivrea-Verbano Zone (IVZ). The IVZ gains this claim from a massive igneous body which intrudes the surrounding paragneiss, providing a glimpse of processes that happen deep within the Earth. The igneous body, known as the Mafic Complex (MC), is thought to be derived from partial melting of the mantle and through its study allows us to investigate the evolution of mafic-ultramafic rocks from an otherwise out of reach component of the Earth. The IVZ is also host to the Kinzigite Formation (KZ), a series of metamorphosed sediments in which the MC is emplaced. Surrounding the KZ are granitic plutons, named Granitoids in this study.

The IVZ has been the centre of numerous investigations due to its petrological significance. Extensive mapping of the IVZ was done by Quick et al. (2003). Geochemical analysis have been performed by Rivalenti et al. (1975, 1980 & 1984), Sinigoi et al. (1994), and Pinarelli et al. (2002). Geochronology dating the IVZ have also been published, e.g.- Peressini et al. (2007) & Pinarelli et al. (1988).

To better understand the IVZ, this study examines in detail hand samples taken from the MC and the Granitoids, as well as their corresponding thin sections. Geochemical data derived from literature is also used to investigative the genesis of these rocks. The aim of this project is to define tectonic settings, magma sources, explore magma evolution, and ultimately investigate if there is a relationship between the various constituents of the IVZ. Any relationships inferred from the results of this study will be beneficial in understanding not only mantle mechanics, but also igneous interactions.

Geological setting

The Ivrea-Verbano zone (IVZ) lies in the Italian alps approximately 100 km northwest of Milan (Fig. 1). It is bounded tectonically in the north and west by the Insubric line, to the east by the Cossato - Mergozzo-Brissago (CMB) Line, and the south by the Cremosina Line (Fig. 1). The Insubric line is the major suture zone that separates the European and Apulian plates. The IVZ, the formations within it, and the sample locations of this study, are defined in figure 1.

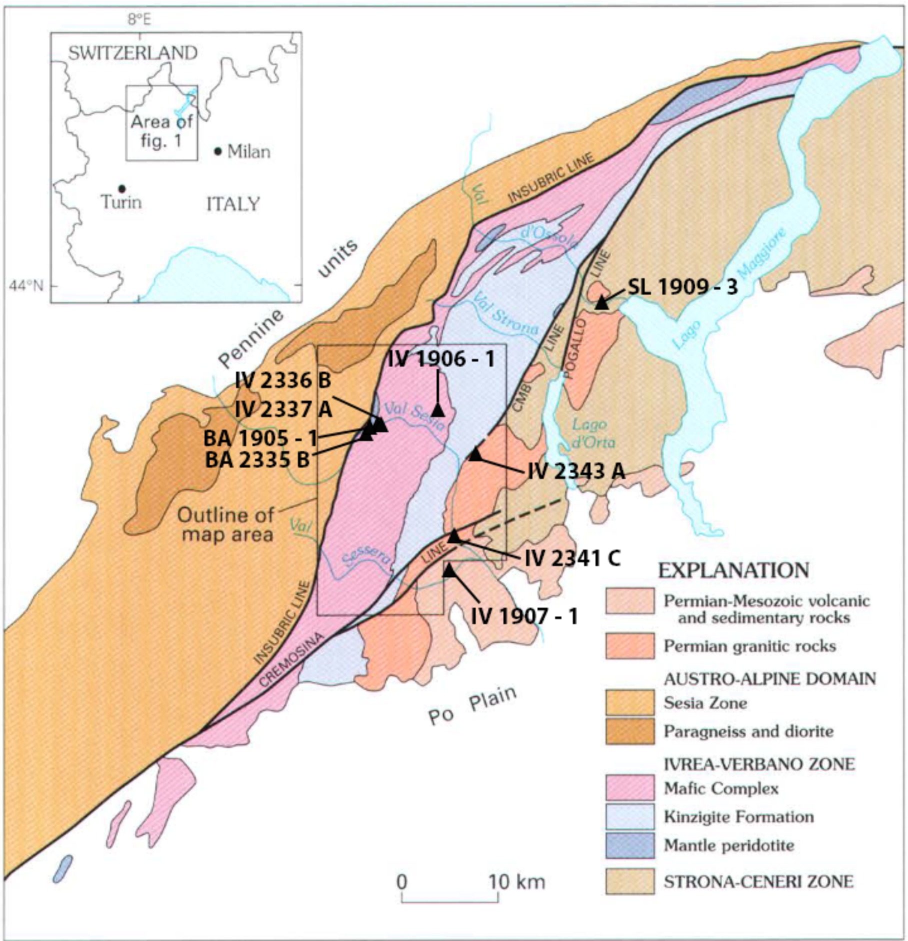

Figure 1. Geology of the southern Alps in the vicinity of the Ivrea-Verbano Zone after Zingg 1980, taken from Quick et al. 2002). The inset shows the location of the study area. Black triangles represent sample locations from this study, along with their identifiers. The box centred on the IVZ is the outline of figure 2.

The IVZ consists of two units, the Mafic Complex (MC) and the Kinzigite Formation (KZ). The MC is an 8 km thick by 35 km wide igneous intrusion that has been exhumed from depths of >15 km and tilted by 90^0 (Peressini et al. 2007). The base and deepest part of the MC borders the Insubric line and consists of granoblastic amphibole-gabbro (Peressini et al. 2007). The roof, representing the shallowest section of the complex, borders the KZ, and is mainly composed of norites, gabbro's and diorites (Peressini et al. 2007). The KZ consists of paragneiss that has undergone amphibolite-facies metamorphism in the eastern IVZ and granitic facies metamorphism in the western IVZ (Peressini et al. 2007).

The age of the MC has been calculated by analysing U-Pb isotopes within zircon. Zircon from the upper MC have a well-defined crystallization age of 288 ± 4 Ma (2σ) (Peressini et al. 2007). The age of the lower MC is not as well-defined, with a large range of ages. The large spread of ages in the lower section is presumed to be a result of inheritance and/or long-lasting periods of zircon growth. Despite this, there are a cluster of ages in the range of 310 Ma, and another between 295 and 285 Ma (Peressini et al. 2007). The age of c. 310 Ma coincides with the age determined for the granulite facies metamorphism of the KZ, however they may not necessarily be related (Peressini et al. 2007).

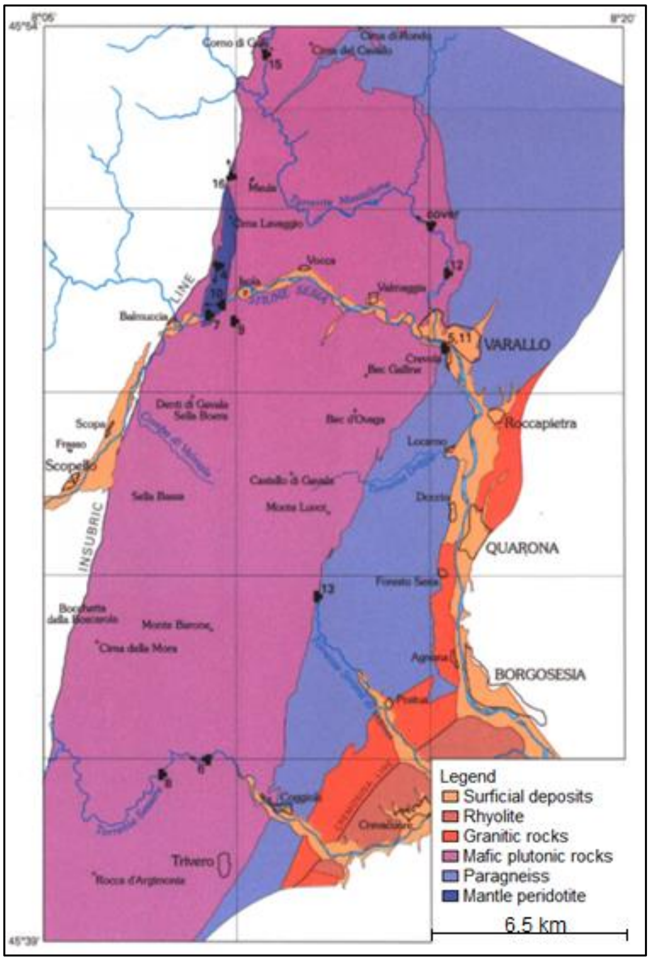

Figure 2. Close-up of the IVZ and generalized geology (after Quick et al. 2002 with the legend redone for clarity).

Methods

Petrography

Ten samples are evaluated for this research project. Key features such as the overall colour, grain size, texture, visible minerals, as well as the rock type are documented (Appendix A, Hand sample descriptions). Each thin section is scanned in both plane polarized light (PPL) and crossed polarized light (XPL) to create an accessible and referenceable archive. The thin sections are described using a petrographic microscope. The mineralogical constituents of the thin sections are identified and recorded, along with their identifying features in both PPL and XPL (Appendix A, Thin section descriptions). Once all minerals are identified, modal abundances for each are calculated using the modal abundance chart from Philpotts (2003). Modal abundances are normalized for the appropriate mineral sets to enable sample classification in accordance with the IUGS systematics of igneous rocks (Le Bas & Streckeisen, 1991). Lastly, the crystallization sequence of the minerals is determined based on visible features within the sections, for example via the presence of inclusions, restrictive growth patterns, and/or replacement processes.

Geochemical data

The geochemical data (23 samples) was mined from the literature. The geochemical data represents two suites, the MC and the neighbouring Granitoids. The MC data comprises analyses from the basal zone (four samples from Rivalenti et al. 1984), the main zone (four samples from Sinigoi et al. 1994), the upper zone (five samples from Sinigoi et al. 1994), and mafic enclaves in diorite from the upper MC (four samples from Sinigoi et al. 1994). The Granitoid data comprises of six samples from Pinarelli et al. (2002).

The samples of Rivalenti (1984) were analysed by an ARL Electron microprobe. Sinigoi et al. (1994) used a combination of methods: the major oxide abundances were calculated by X-Ray Fluorescence (XRF), and the rare earth elements (REE) were measured with either inductively coupled plasma mass spectrometry (ICPMS) or spark source mass spectrometry (SSMS). Data from Pinarelli et al. (2002) was also obtained with XRF for the major oxides and the REEs were obtained using ICPMS. Geostandards were stated to have been used by Pinarelli et al. (2002), and Sinigoi et al. (1994).

These data were inspected for quality (totals 100±2 wt%), suitability (appropriate trace elements recorded), and normalized to 100% dry totals before plotting. Rock names are determined using the total alkali verses silica (TAS) diagram, Harker diagrams are plotted to observe trends in magma evolution, and later explored via the use of Pearce element ratio (PER) diagrams. Multielement diagrams are constructed from the trace element data for mantle source determination. Tectonic discrimination diagrams are selected on a basis of suitability and reliability as reported by Rollinson & Pease (2021) and determined by references therein (Vermeesch 2006a, Verma et al. 2013).

Results

The petrographic assessment summarizes key findings with respect to mineralogy (Figs. 3-6). The modal plots detail sample names (Fig. 7). The geochemical data is used to investigate possible crystal fractionation sequences, magma evolution and tectonic origins. The major oxides are plotted in a total alkali verses silica diagram (TAS) (Fig. 8) and Harker diagrams (Fig. 9). The trace element data has been potted as multielement diagrams for both the MC (Fig. 10) and Granitoids (Fig. 11).

Appendix A comprises of the complete ten petrographic descriptions and modal analysis of the various thin sections from the IVZ that were assessed within this study, as well as the large cropped thin section scans. Appendix B contains the mined data from the literature, presented in table B1 for the Mafic Complex data and table B2 for the Granitoids. Within the tables is the assigned identifier (ID), TAS name, data origin, method of data acquisition, major elements in weight percent (wt %) and trace elements in parts per million (ppm).

Petrography

Thin section summary:

BA 1905 – 1 is a section of a pyroxene rich vein intruding the olivine websterite host rock, identified with help of the hand sample. The vein can be seen clearly in PPL as the green colour is distinct (Fig. 3). Pigeonite exsolution is also seen, represented by the parallel streaks within pyroxene (Fig. 3).

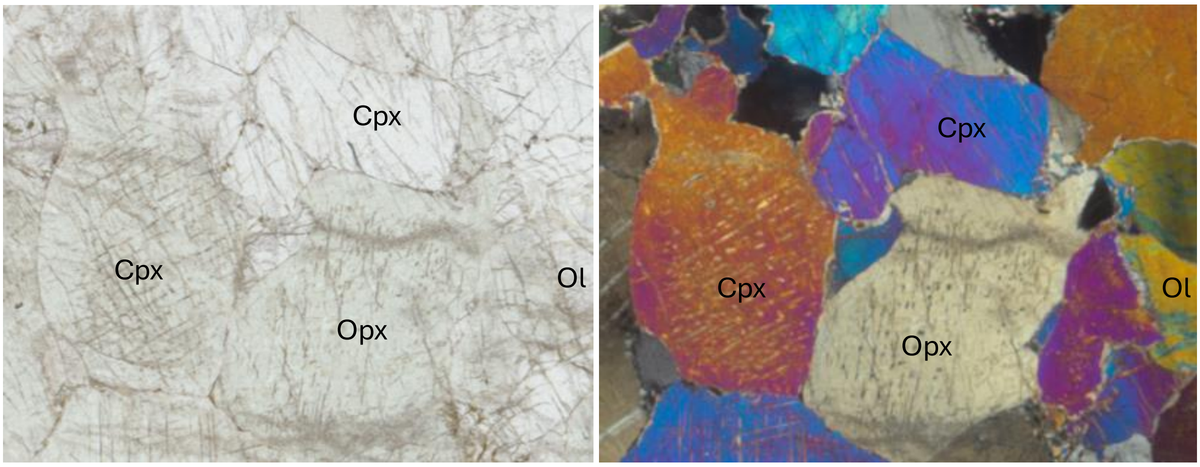

Figure 3. BA 1905 – 1 in PPL (left) and XPL (right), field of view is 0.36 mm. Pictured is the distinct green that the pyroxene rich vein exhibits (bottom of left image) contrasting with the host rock which lacks the green tint (top of left image). Pigeonite exsolution is seen in clinopyroxene. Olivine is seen in the right of the frame.

BA 2335 – B has cumulus olivine with regions rich in spinel and clinopyroxene (Fig. 4). The spinel is seen in both hand sample and thin section, and clinopyroxene has pigeonite exsolution (not shown). Pigeonite exsolution is also found in thin sections BA 1905 – 1 (Fig. 3), IV 1906 – 1 and IV 2337 – A.

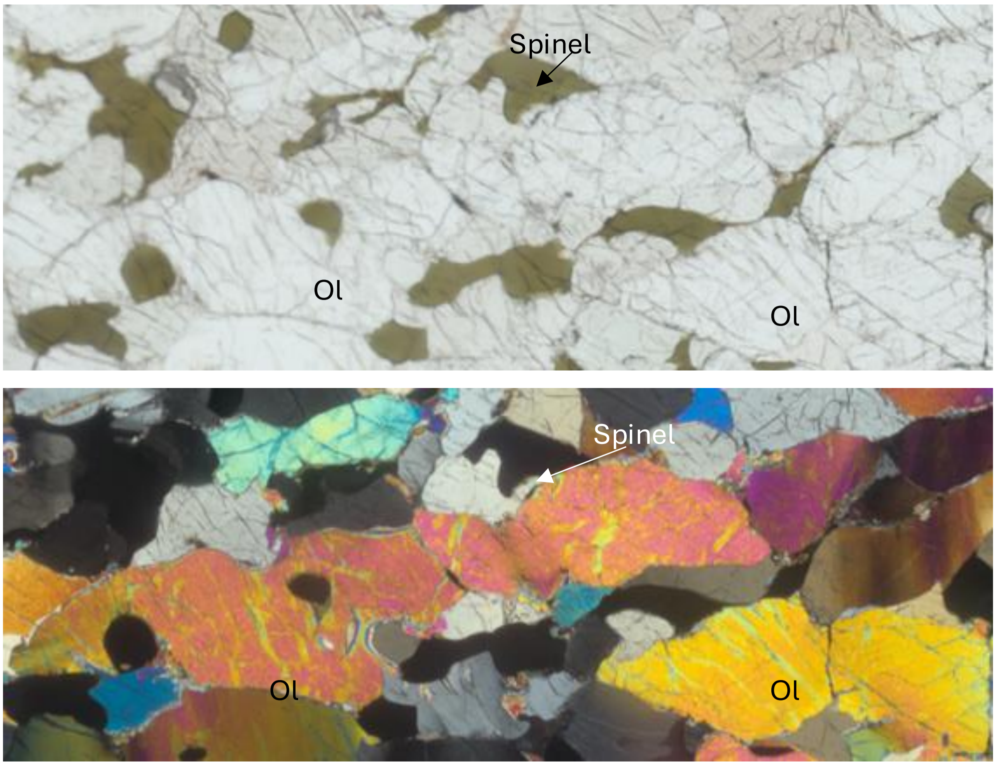

Figure 4. BA 2335 – B in PPL (left) and XPL (right), field of view is 4 mm. This photomicrograph depicts cumulus olivine with intertwined spinel.

IV 2336 – B (figure 5) is centred over a serpentinized fracture, with numerous brittle features cutting the surrounding crystals. Several serpentine filled fractures are identifiable in hand sample. Despite this, serpentinization of olivine minerals was not pronounced in any of the samples.

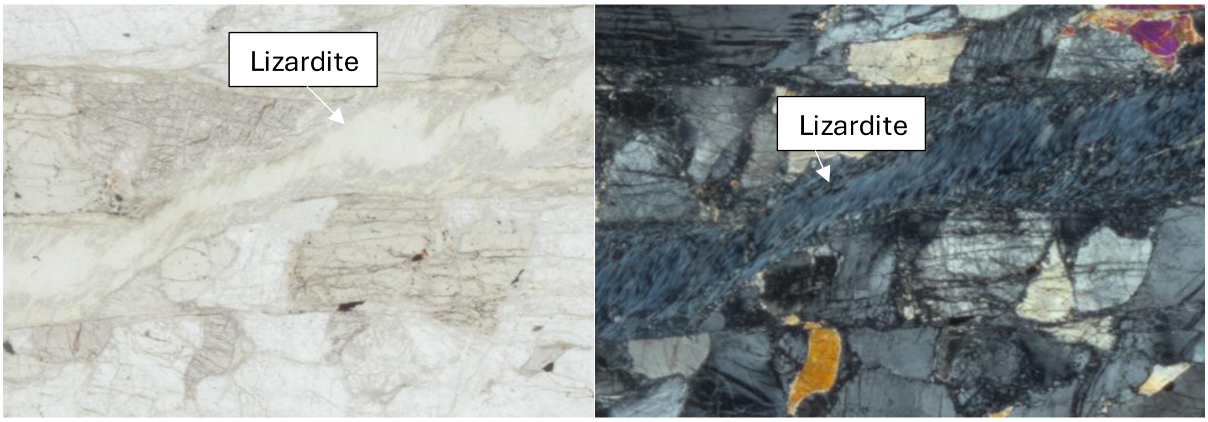

Figure 5. IV 2336 – B in PPL (left) and XPL (right), field of view is 0.42 mm. The serpentine mineral found within the vein is presumed to be lizardite due to its yellow colour. Also pictured are brittle features extending from the vein, splitting the host rock's pre-existing pyroxene crystals.

All samples containing plagioclase (IV 1906 – 1, IV 2336 – B, IV 2341 – C, IV 2343 – A & SL 1909 – 3) were saussuritized - see the example presented in figure 6 from sample IV 2343 – A.

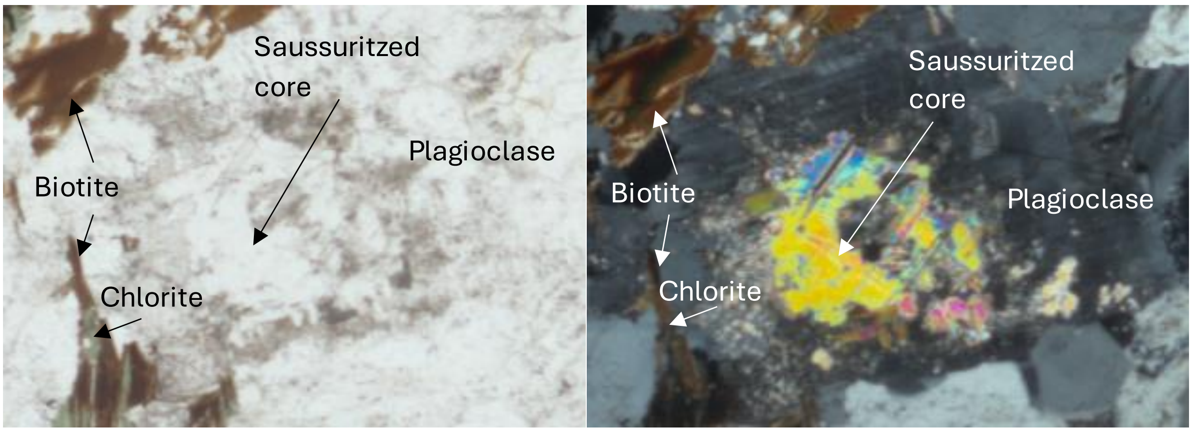

Figure 6. IV 2343 – A in PPL (left) and XPL (right), field of view is 0.42 mm. Photomicrograph showing a saussuritzed plagioclase. Also seen is biotite (brown, PPL & XPL) and chlorite (green, PPL)

In all the mafic rocks, excluding IV 2336 – B, spinel was present in quantities varying from <1% to 15%, as can be seen throughout appendix A.

Rock types:

According to the IUGS mode, MC samples represent websterite, olivine websterite, gabbro, and olivine gabbro (Fig. 7). The Granitoids represent granodiorite, granite, and alkali feldspar granite (Fig. 7).

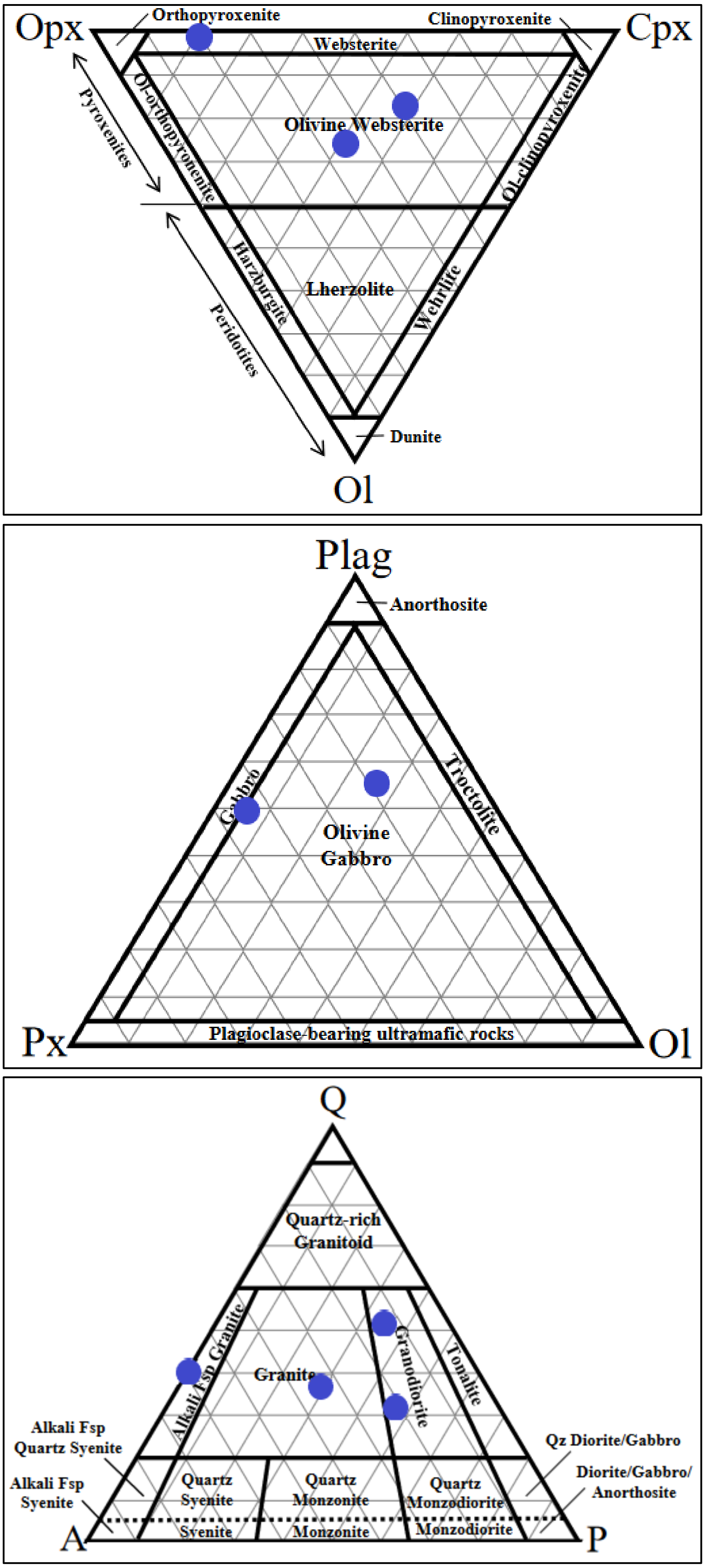

Olivine Websterite	
BA 1905 – 1	BA 2335 – B
Websterite	
IV 2337 – A	

Olivine Gabbro	
IV 1906 – 1	IV 2336 – B

Granodiorite	
IV 2341 – C	IV 2343 – A
Granite	
SL 1909 – 3	
Alkali Feldspar Granite	
IV 2340 – B	

Figure 7. Ternary plots of the nine thin sections according to their modal abundance. Thin section ID are reported for each ternary plot with their respective IGUS rock names.

Geochemical data

Major oxides

A TAS diagram is plotted from the gathered geochemical data (Fig. 8). Most of the MC suite plot in a gabbro field, ranging from foid-, peridotite-, alkaline- and subalkaline- with the more evolved samples being in the monzonite section. The granitoids are all subalkaline, with two in the quartz monzonite field and the rest residing within the granite field. When the MC is separated into its respective zones, (basal, main, upper, enclaves) the same rock unit plots in both alkaline and subalkaline fields as can be seen in table B1. For the granitoids, the quartz monzonite is not unique to one locality, as can be seen in table B2. An AFM diagram (not included) distinguishes that the MC alkaline rocks have a tholeiitic trend.

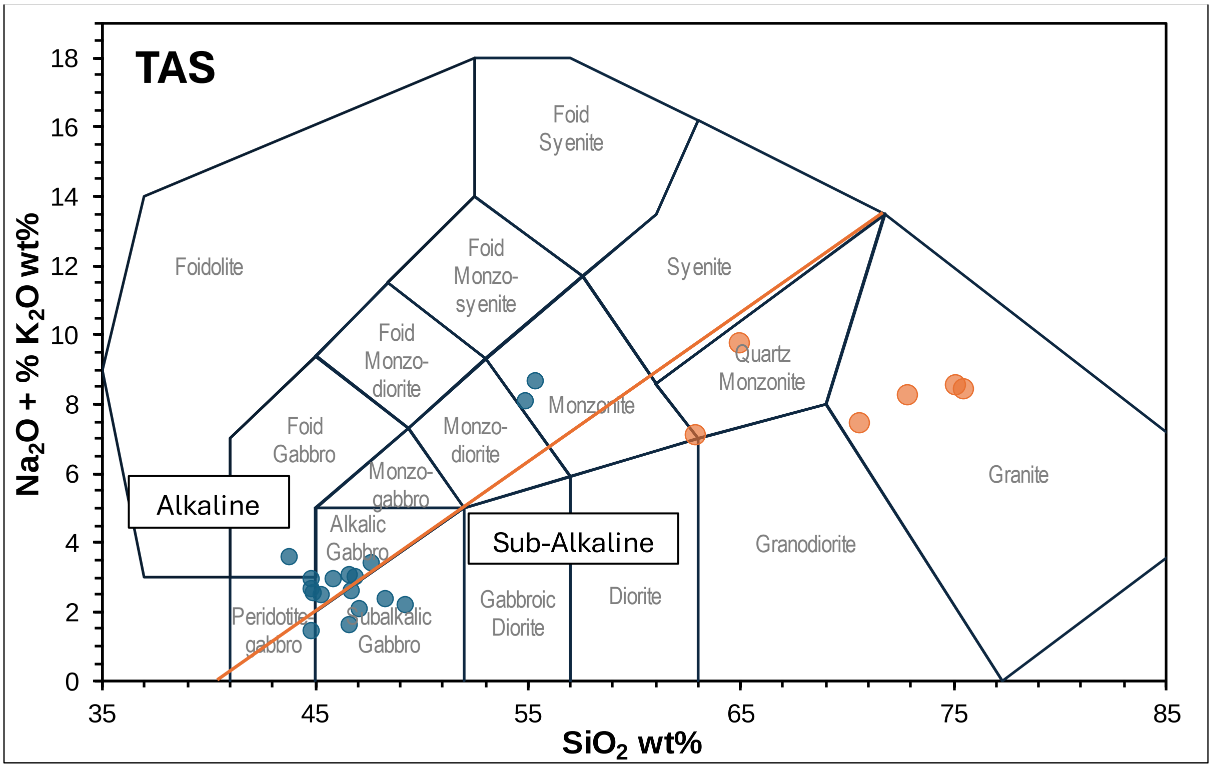

Figure 8. Total Alkali verses Silica diagram of the geochemical data on the suite of samples from the Mafic Complex (blue circles) and the Granitic rocks (orange circles). There is a mix of both alkaline and sub-alkaline rocks within the MC and the Granitoids are all sub-alkaline.

Harker diagrams (Fig. 9) show a decrease of Mg and Fe with respect to Si in the MC. Al increases as you progress up from the basal zone to the upper zone. Vertical scatter is present in the plots of Al, Mg, Fe, Ti, and P. These patterns may reflect potential fractional crystallization process.

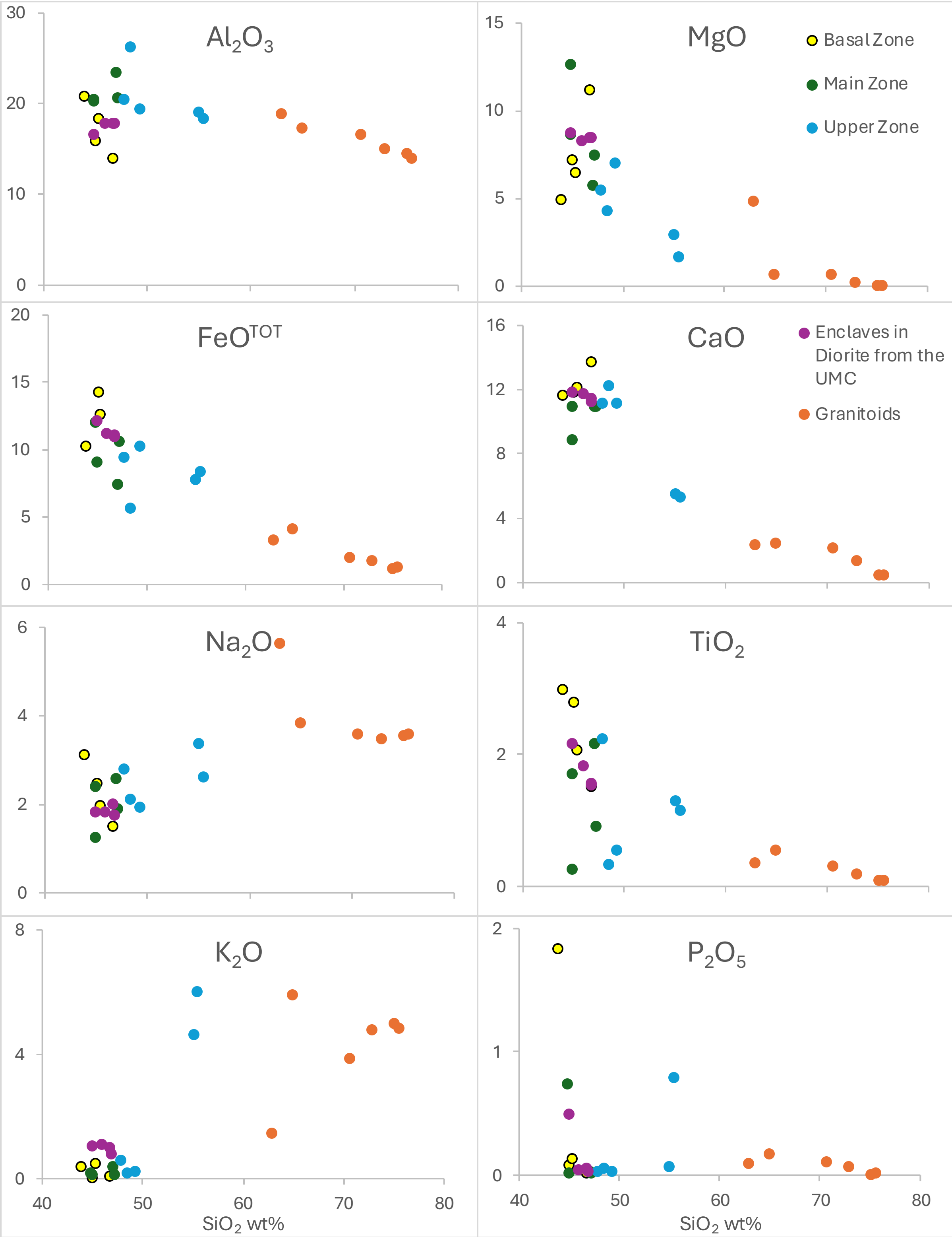

Figure 9. Set of Harker diagrams for both the Mafic Complex (yellow, purple, green, and light blue circles) and the Granitoid (orange circles) compositions. All scales are in weight percent and data has been normalized to 100%. Note the large vertical scatter in the MC component of the various diagrams. At 45 wt% SiO_2, Al_2O_3 ranges from 14 to 23.5 wt%, MgO varies from 6.5 wt% to 12.6 wt%, and TiO_2 varies from 0.2 to 2.8. This vertical scatter persists internally within the basal, main, and upper zones of the MC.

Trace elements

Mafic Complex

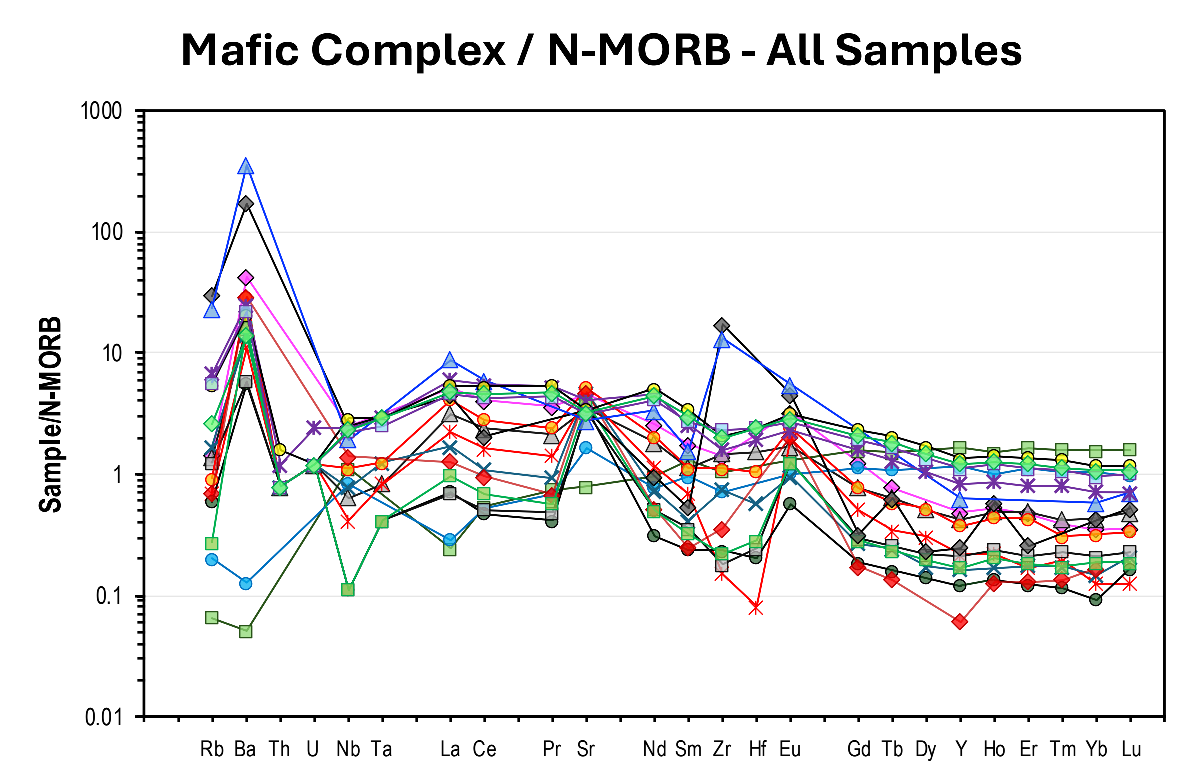

Figure 10. Multielement diagram of all the MC samples normalised to N-MORB (Sun & McDonough 1989).

From the MC multielement diagram (Fig. 10) the overall trend of the trace elements is seen. Noteworthy are the two Monzonites (Blue triangle - UZ 5 and black diamond – UZ 4) that are both rich in Ba and Zr, with the latter indicating contamination from crustal material. The two samples low in Ba (Blue circle – BZ 4, green square – BZ 2) are both from the basal zone and go against the overriding trends (opposite La/Yb ratio, low Rb, low Ba, low La, high Lu). In the absence of these four samples coherent trends are evident, therefore the samples BZ 2 & 4 and UZ 4 & 5 will be excluded from the interpretations, to provide a representation of a typical MC sample.

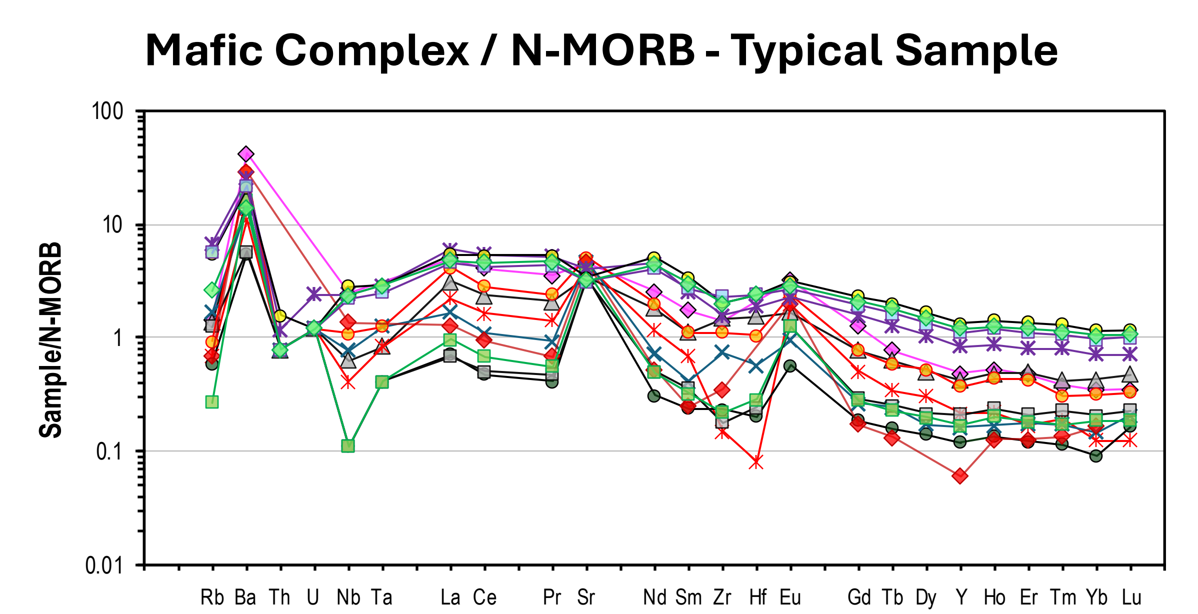

Figure 11. Multielement diagram of the MC normalised to N-MORB (Sun & McDonough 1989). Samples BZ 2 & 4 and UZ 4 & 5 have been removed to provide a clear picture of the trace element trends throughout a typical sample of the MC.

Figure 11 excludes these problematic samples and better represents typical MC samples. There is enrichment of the large ion lithophile elements (LILE) group compared to N-MORB; Ba has values ranging from 4 to 40 sample/N-MORB (with samples BZ 2 & 4 and UZ 4 & 5 excluded); Sr has values ranging from 3 to 4 times N-MORB concentrations; Eu has a positive anomaly and values ranging from 0.5 to 3 times N-MORB; La has values between 0.7 to 5 sample/N-MORB (with samples BZ 2 & 4 and UZ 4 & 5 excluded).

The high field strength elements (HFSE) show N-MORB like to gradual depletion concentrations; Nb has sample/N-MORB values ranging from 0.1 to 2.8; Ta values range from 0.4 to 3 when compared to N-MORB; Zr values are between 0.2 to 2 sample/N-MORB (with samples MC 12 &13 excluded); Hf has values ranging from 0.1 to 2.4 sample/N-MORB.

The heavy rare earth elements (HREE), which are those from Eu until Lu are depleted with respect to N-MORB, apart from Eu as there is a positive Eu anomaly present in these samples. The values (sample/N-MORB) for the HREE range from the lightest, Gd (Eu excluded) at 0.2 to 2 through to the heaviest, Lu at 0.1 to 1 (sample BZ 2 excluded)

The average $(La/Yb)_n$ ratio of the MC samples (with samples BZ 2 & 4 and UZ 4 & 5 excluded) is 7.39. The lowest ratio being sample MZ 4 with a value of 2.90 and highest being sample MZ 1 with a value of 15.57. The average $(Ho/Lu)_n$ ratio for the typical MC sample is approximately 1.28, with the highest value at 1.95 (sample MZ 1) and lowest 0.90 (sample MZ 2 & 3).

Granitoids

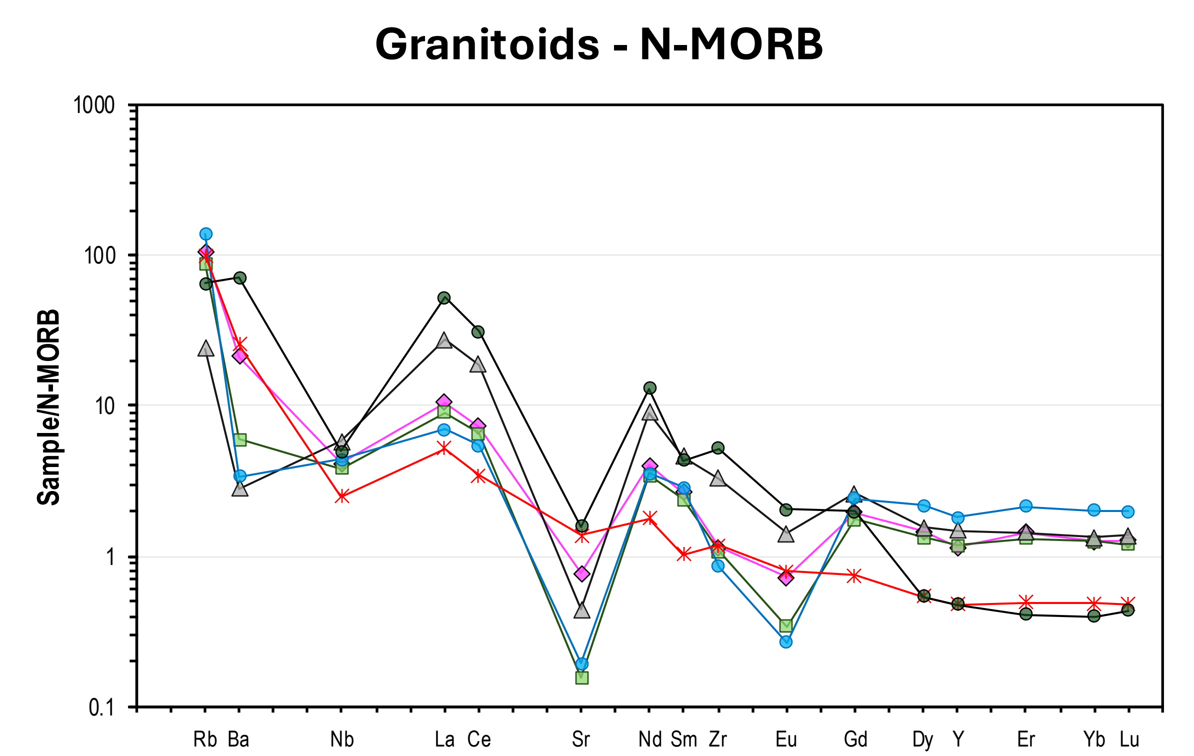

Figure 12. Multielement diagram of all granitoid samples compared with N-MORB (Sun & McDonough 1989).

With the exception of two samples from Alzo Roccapietra (Samples G 5 & 6), the granitoid samples define a consistent pattern (Fig. 12). They show significant enrichment in some of the LILE for the when compared to N-MORB; Ba values are between 2.8 to 71; La has values ranging from 5.3 to 52.3; Sr and Eu however have negative anomalies, with values ranging from 0.2 to 1.6 for Sr and 0.3 to 2 for Eu. The HFSE show moderate enrichment compared to N-MORB; Nb has values ranging from 2.5 to 5.0; Zr values are between 0.9 to 5.2. Unlike the MC, the Granitoids HREE pattern show slight enrichments. Typical HREE/N-MORB values range for Gd between 1.8 and 2.5 and Lu values are between 1.4 and 2.0.

The Alzo Roccapietra samples (G 5 & 6) are comparatively depleted in the HREE with values in the range of 0.4 to 0.5 HREE/N-MORB. The Alzo Roccapietra samples also possess very moderate Sr and Eu negative anomalies in comparison to the other Granitoids.

Discussion

Combining the petrographic observations with REE data, the magma source(s), depth of melting, and tectonic environment(s) are considered. From petrological observations and major oxide data, the magmatic evolution of the MC is evaluated from the perspective of crystal fractionation, crustal assimilation, and rejuvenation. The MC and the Granitoids are then discussed in relation to the surrounding Kinzigite formation, in which simple binary mixing models are used to determine if a link exits between the MC, Granitoids, and/or the surrounding Kinzigite formation.

Mafic Complex magma evolution

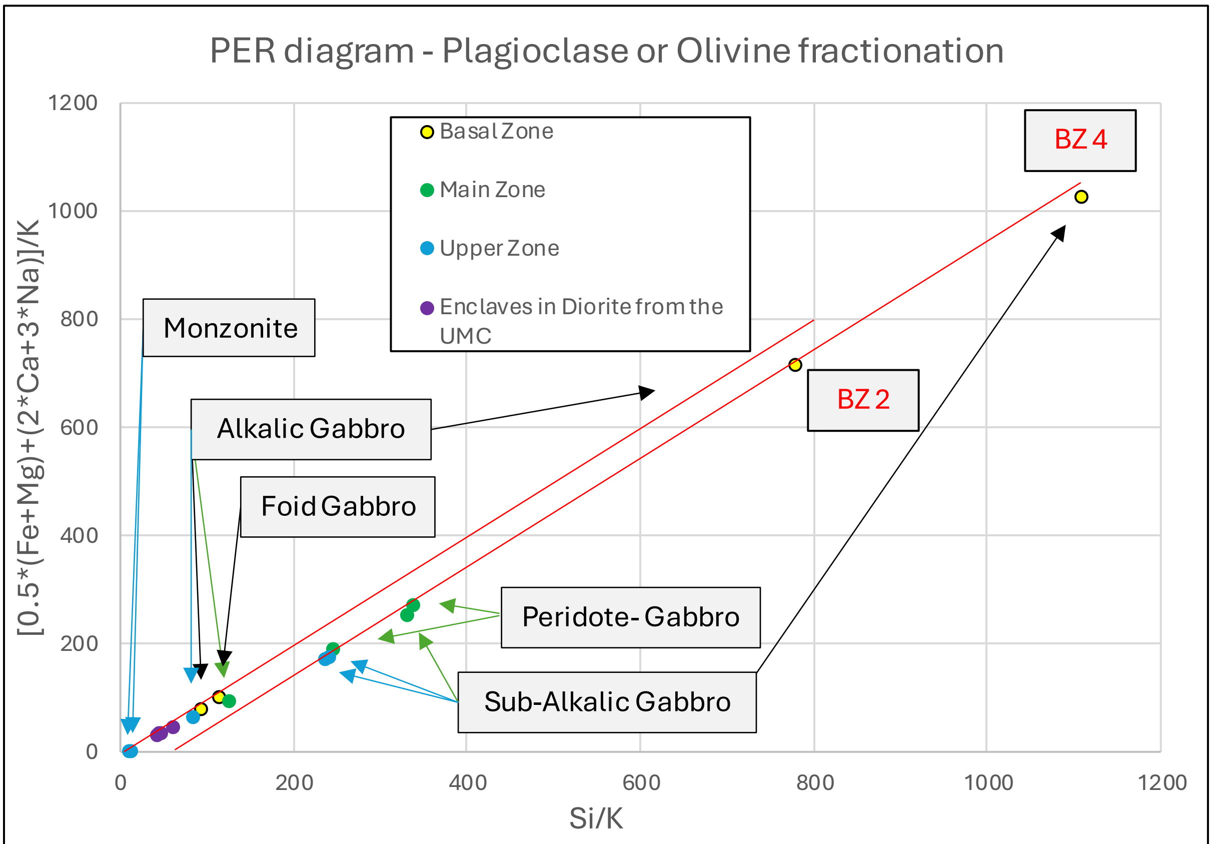

Figure 13. PER diagram of Plagioclase and / or Olivine fractionation. Olivine will remove Fe and Mg ions at a rate of 2:1 to Si, therefore their equation is 0.5*(Fe + Mg) to keep a slope of 1 with respect to Si. Plagioclase removes Ca and Na in ratios 1:2 and 1:3 to Si, respectively, therefore their equation is (2*Ca + 3*Na) and should have a slope of 1 with respect to Si. K is a conserved element; therefore, all axes are divided by K to give a proportionate ratio. Samples that plot on a slope of 1 may fulfil the criteria for magma evolution by plagioclase and/or olivine fractionation.

To test different crystal fractionation hypotheses, Pearce Element Ratio (PER) diagrams are used (after Pearce, 1968). PER diagrams compare elemental ratios based on quantities of elements removed via different fractionations. From figure 13, two fractionation trends can be defined, indicated by thin red lines; both lines have a slope of 1 with respect to Si. One fractionation trend is defined by the Enclaves in Diorite from the UMC and the basal zone consisting of alkalic samples - it passes through the origin at 0.0 and has a slope of 1. The second fractionation trend is represented by the samples from the Upper Zone and the Main zone, and it too has a slope of 1, although the y-axis intercept does not intersect at the origin which implies another process in addition to the crystal fractionation. Two separate trends suggest that there are two magma series, and that Plagioclase and/or Olivine fractionation played a role in the evolution of them.

Samples BZ 2 & 4 (marked in Fig. 13) were two of the four samples excluded from the typical multielement plot (Fig. 11) as they did not have the overriding MC trace element trends. These samples have very high ratios (~700s and 1000+, respectively) due to having minute quantities of K_2O (0.04 and 0.06 wt%, respectively) and therefore a low denominator in the PER calculation. Although they appear to reside on the Main and Upper zone trend, this result cannot be relied upon as even a small analytical error will shift these samples on the plot dramatically.

The two Monzonites from the Upper Zone, samples UZ 4 and UZ 5, were the other two samples excluded from the multielement plot. These two samples have the highest K content of the MC (4.58 and 5.97 wt%, respectively), whereas all other MC samples are in the range of 0.1 to 1.1 wt% (excluding samples BZ 2 & 4 as the lower outliers). Their very high K content gives them a large denominator in the PER calculation, which makes them plot very close to the origin.

The Alkalic-Gabbro samples from the main zone (MZ 3) and from the upper zone (UZ 1) appear to plot near the Basal and Enclaves trend. Looking at probable causes as to why these two samples plot on the basal trend and not the main and upper trend, sample MZ 3 has a K_2O content of 0.38 wt% which is double that of the next richest main zone sample, MZ 1 at 0.18 wt%. The same can be said about sample UZ 1, which has a K_2O = 0.57 wt%, whereas the other upper zone samples (excluding UZ 4 & 5 as already discussed) have K_2O values of 0.20 & 0.21 wt%.

K_2O was chosen as the common denominator as it is a conserved element in the crystal fractionation of plagioclase and olivine. K_2O concentrations therefore should only increase in proportion as the melt evolves and other phases decrease in proportion. However as demonstrated by samples MZ 3 and UZ 1, 4 & 5, abnormally high K_2O concentrations can skew the calculated ratios, while abnormally low K_2O concentrations can drastically increase the calculated ratios, as demonstrated by samples BZ 2 & 4.

Olivine fractionation agrees with the petrographic results where cumulate olivine textures are observed. Cumulates form from minerals settling or floating out of a melt. In the case of olivine, crystals will settle as olivine is typically denser than a gabbroic melt, thus it should be found in larger quantities at the base of the MC. Samples BA 1905 – 1, BA 2335 - B, and IV 2336 - B are all from the base of the MC, as can be seen in figure 1, where further west is equivalent to deeper in the crustal section; these samples have significant olivine concentrations (18%, 22.5%, 25%, respectively). IV 2337 - A is the exception with a low amount of olivine (2.5%) and comprised almost entirely of pyroxenes (82%). Sample IV 1906 – 1 which lies further east and therefore higher in the complex, only has 5% olivine.

Plagioclase cumulates are not seen in the thin-sections that hosted plagioclase (IV 1906 – 1, IV 2336 – B, IV 2341 – C, IV 2343 – A & SL 1909 – 3), and therefore cannot be used to confirm plagioclase fractionation. Plagioclase, unlike olivine, is lighter than a gabbroic melt, and therefore should float upward in a gabbroic system. It can be assumed that rocks higher in the MC would have greater plagioclase concentrations however a significant difference was not found. IV 1906 – 1 has approximately 44% plagioclase, whereas sample IV 2336 - B (a sample lower in the MC) has 52% plagioclase. The positive Eu anomaly in the multielement diagram constructed from the geochemical data (figure 11) is indictive of plagioclase fractionation and therefore allows plagioclase fractionation to be an acceptable assumption.

As shown in figure 13, two fractionation trends are indicated. These separate trends can be explained via magma refertilization/recharge, a process of hotter and more primitive magma entering the reservoir and thereby rejuvenating it. This process would explain the horizontal shift in depleted elements and thereby the ratios in figure 13, as all elements become replenished. The same fractionation then continues and that is why the samples plot along the same slope, but a different trend. Petrographically, this is seen in samples 1905 – 1 (figure 3), IV 2335 – B (figure 4) and IV 2337 – A. Sample 1905 – 1 has the distinct pyroxene-rich green vein, IV 2335 – B has the pyroxene spinel-rich veins and finally, IV 2337 – A is the Websterite, a rock made up almost entirely of pyroxene and is now suggested to be the result of this rejuvenation event. From the set of Harker diagrams in figure 9, refertilization could explain the observed vertical scatter of many elements at the same SiO_2 concentrations.

In the context of magma refertilization, plagioclase fractionation is instead suggested to be removed from the system and to not accumulate within the MC. The composition of the rejuvenation veins in the MC lacks both olivine and plagioclase, this suggests that the source of the rejuvenation also underwent plagioclase and olivine fractionation. Given that the MC multielement plot (Fig. 11) has the same overall pattern (suggesting a similar source), it seems likely that the rejuvenation in the main and upper zone came from the basal zone.

Kinzigite Formation, the Mafic Complex and the Granitoids

The Kinzigite Formation (KZ) which is made up of paragneiss is divided into two sections, the western part where the formation has undergone granulite facies metamorphism (Granulites) and the eastern part where the formation underwent amphibolite facies metamorphism (Amphibolites). Peressini et al. (2007) and references therein state that the bulk composition of the granulite paragneiss can be explained by the removal of 20-40% partial melt from a protolith composition much like the amphibolite paragneiss. Assuming that the Granulites were formed via a melt extraction from the Amphibolites and using average compositions (major oxides and trace element data) for the Granulites and Amphibolites from Schnetger (1994), possible correlations between the MC and the Granitoids are explored. To best represent the MC, the Enclaves in Diorite from the UMC were used - they are interpreted to be the least contaminated and therefore the most pristine (least modified) endmember. Selection of suitable elements to plot is based on the expected behaviour of incompatible elements during anatexis. Using these criteria and assumptions, simple binary mixing comparing the Granitoids, the MC and the surrounding Kinzigite formation was explored (Fig. 14).

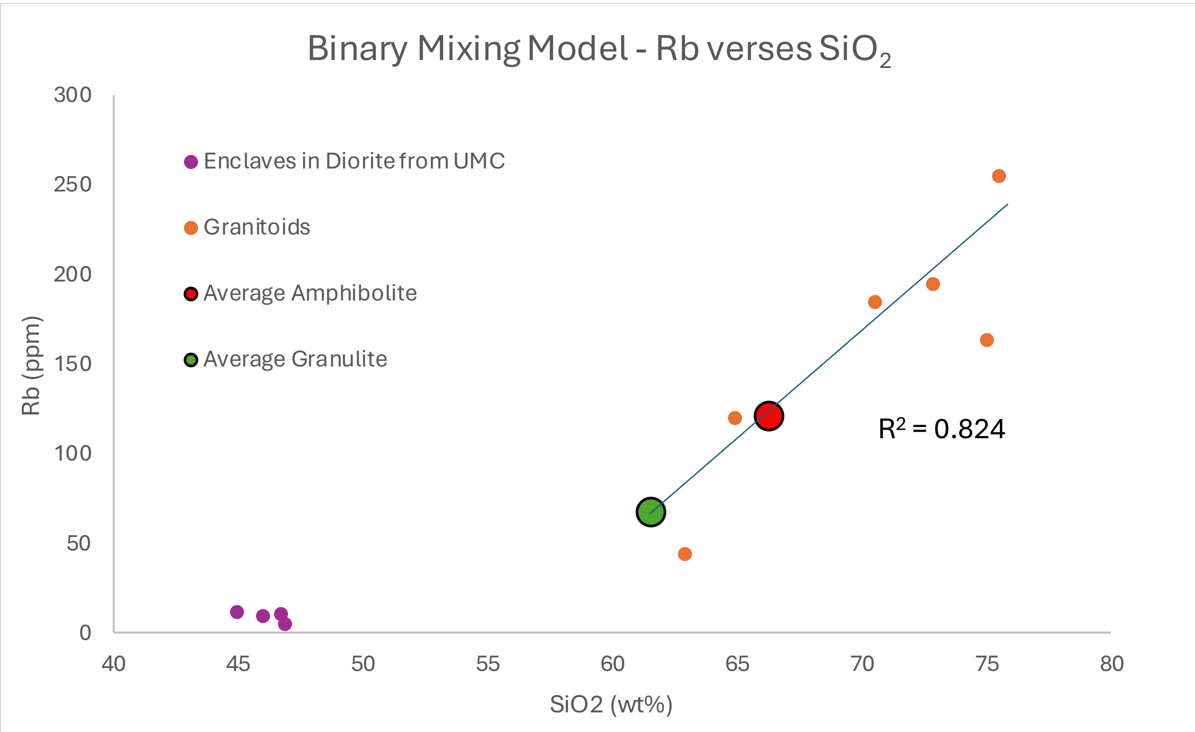

Figure 14. Binary mixing model comparing the KZ with the MC and Granitoids. The compositions of the granitoids and the Enclaves in Diorite from the UMC are plotted. The average amphibolite and granulite compositions of the KZ are shown (from Schnetger, 1994). The R^2 value (0.824) for a mixing line between the KZ (both the average amphibolite and average granulite facies) and the Granitoids is indicated.

In figure 14, the amphibolite facies paragneiss and the granulite facies paragneiss are plotted as large green and red circles, respectively. The element chosen to represent a potential binary mixing was Rb, as it is an incompatible element and will be concentrated in the melt during partial melting. Rb should therefore increase in concentration with an increase to silica, as is seen. A mixing line joining the average Amphibolite to the average Granulite paragneiss and extrapolated to higher silica, intersects the Granitoid field. There is therefore a possible correlation between the KZ and the Granitoids based on this binary array. Unlike the Granitoids, the MC does not fit on this trend, suggesting that it is unrelated to the gneiss of the KZ and Granitoids via simple binary mixing. Other typically incompatible elements also tested for a binary correlation, such as Zr and Sr, but they increase as silica decreases. A decrease in incompatible elements with increasing silica suggests other factors at work and requires further investigation.

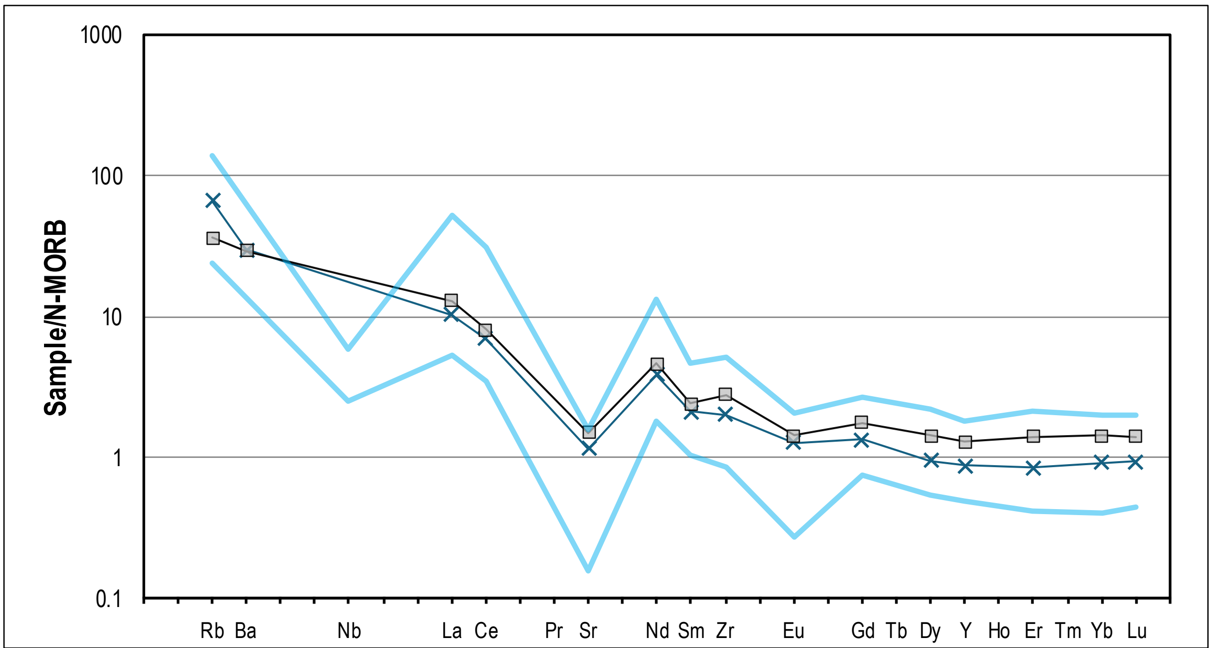

Figure 15. Multielement plot of Granitoids and Amphibolites. Maximum and minimum REE values of the Granitoids normalized to N-MORB are the light blue lines, Amphibolite data is the darker blue line with crosses and the Granulite data is the light grey squares. Note the similarity of their N-MORB normalized REE patterns.

Due to the observed correlation between certain elements, a multielement diagram comparing the Amphibolites and Granulites to the Granitoids was constructed (Fig. 15). The Amphibolites and Granulites plot within and follow the overall trend of the Granitoids.

Magma origins

Mafic Complex

Magma sources can sometimes be inferred from their element patterns. Incompatible elements are expected to behave similarly. Both the large ion lithophile elements (LILE) and the high field strength elements (HFSE) are considered incompatible, however LILEs are more soluble in H_2O than HFSEs (Winters 2014). the relative enrichment of N-MORB normalized LILEs relative to the depletion of the N-MORB normalized HFSEs is termed 'decoupling'. In a subduction zone, H_2O will be trapped within the subducting plate. The slab dehydrates as it is subducted to greater depths and higher temperatures, releasing H_2O into the wedge of mantle above it.

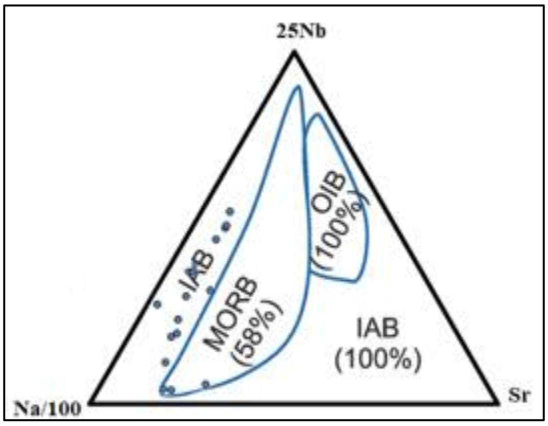

Figure 16. Discrimination diagram of the MC (after Vermeesch, 2006a). The MC geochemical data plots within, or on, the borders of the island Arc Basalt section. The other two sections labelled are the Mid-Ocean Ridge Basalt (MORB) and Ocean Island Basalt (OIB).

To test the theory of a subduction related origin for the MC rocks, the tectonic discrimination diagram is shown in figure 16. The selection of the diagram was based on correct classification percentage of specifically subduction type settings, and the available geochemical data. Figure 16 (after Vereesch 2006a) uses the elements Na, Nb and Sr to discriminate between Mid Ocean Ridge Basalts, Ocean Island Basalts, and Island Arc Basalts. The samples (Blue circles) reside in, or on the margins of, the Island Arc Basalts section.

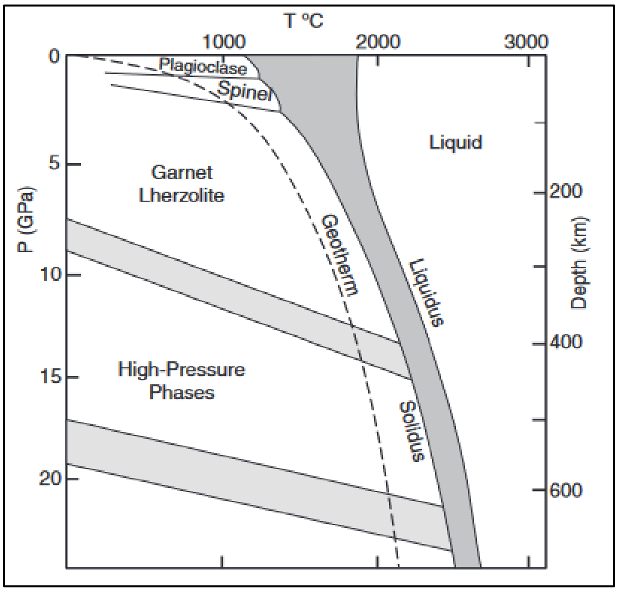

Figure 17. Taken from Winters (2014), showcasing the different mineral phases present at different depths within the mantle. From this, we can see that there are three minerals that are indicators of depth, garnet, spinel, and plagioclase.

The depth of the magma source is considered in figure 17. There are three minerals distinctive for mantle source region: garnet, spinel, and plagioclase. HREE are predominantly incompatible elements and many of the major rock building mineral phases do not include them. There is an exception with garnet, which instead has a high affinity for HREEs; it has a distribution coefficient of 11.5 and 11.9 for Yb and Lu, respectively (Winters, 2014). Much like as the previously discussed decoupling between HFSE and LILE, garnet will decouple the HREE from the other REEs. When a magma forms at the depth of garnet stability, there will be depletion of Yb and Lu as these are retained in garnet, and this is represented by a greater than 1 $(Ho/Lu)_N$ ratio. The calculated average $(Ho/Lu)_N$ ratio for the typical MC is 1.30 therefore garnet fractionation did occur.

From the petrographical investigation, remanent pigeonite features within pyroxenes are present (see Appendix A; BA 1905 – 1, IV 1906 – 1 and IV 2337 – A, for examples from the thin section scans). Pigeonite, which is in essence a combination of both clino- and orthopyroxene, can only exist under high temperatures. As temperatures lower, pigeonite will invert to enstatite and expel augite as lamella. Figure 18 visualizes this compositional region, highlighting the miscibility gap of pigeonite. From this figure, pigeonite requires temperatures greater than 1150 °C to form, otherwise no exsolution lamellae would be present.

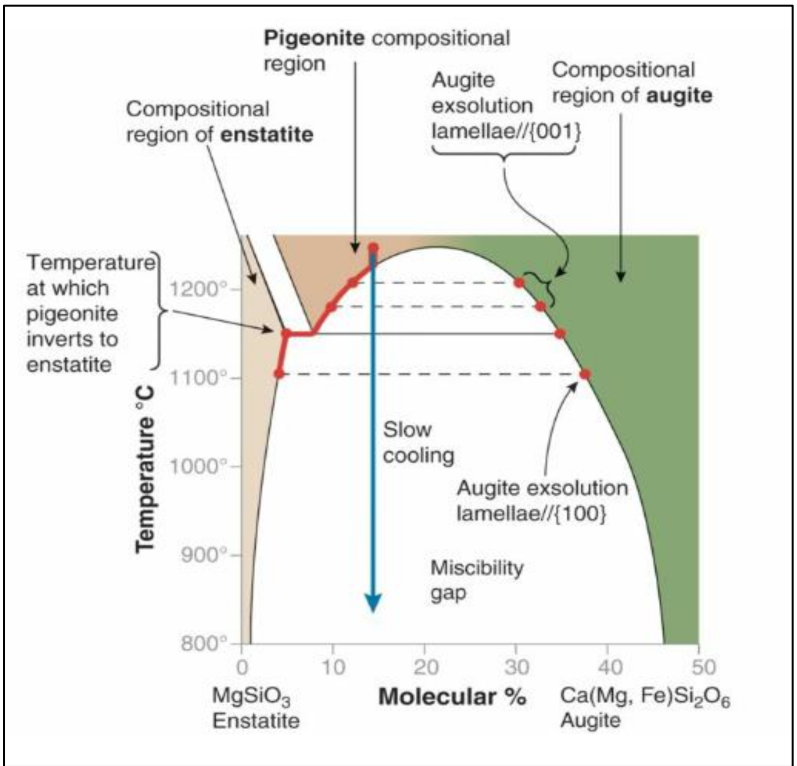

Figure 18. A diagram taken from Klein & Philpots (2017) detailing the range for pigeonite stability. Note the inability of pigeonite to exist below temperatures of 1150°C.

Finally, spinel was a common accessary mineral found in the mafic thin sections. Spinel also requires at least 1150 °C, and together with the garnet HREE signature, implies that the magma source was from the garnet zone. The garnet zone is at depths greater than 80 km (Winters, 2014).

Granitoids

Figure 19 is a discrimination diagram created to test the relationship between the granitoids and their formative tectonic environment. Figure 19 was the selected discrimination diagram based

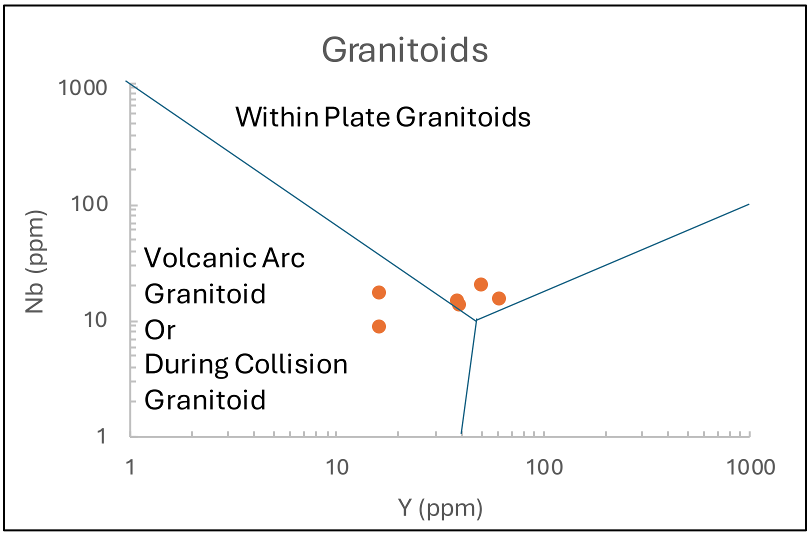

Figure 19. Tectonic discrimination diagram of the Granitoids (after Pearce et al. 1984) with selection based on available geochemical data as well as acceptable classification rates after Verma et al. (2013). The two samples in the volcanic arc/collision area are G 5 & 6 and are from Alzo Roccapietra.

on the available geochemical data and by classification accuracy as determined by Verma et al. (2013). From Figure 19, there is a difference between the granitoids from Alzo Roccapietra and the other four within-plate granitoid samples. The Alzo Roccapietra samples, samples G 5 & 6, are depleted in HREE compared to N-MORB and the other granitoid samples in the multielement diagram (Fig. 12). As well as being depleted in HREE, the Alzo Roccapietra samples have weak negative Eu and Sr anomalies, suggesting that the Alzo Roccapietra pluton originated at a slightly greater depth. This may explain why they plot distinct from the other four Granitoid samples (G 1 – 4) in the within-plate filed.

From the section on the Kinzigite Formation above, a potential correlation between the KZ and the Granitoids is suggested. Placing this relationship in the context of Carboniferous orogenesis and the formation of the European Alps, the Granitoids could be the result of post-orogenic decompression melting. This could explain their separate trace element pattern from the MC and the apparent relationship with the KZ.

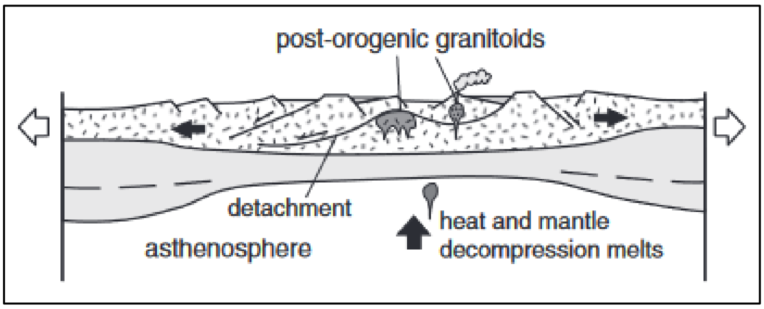

Figure 20. Schematic representation of post-orogenic decompression melting (after Winters, 2014). White arrows on the side indicate relaxation of tectonic compressional forces. Black horizontal arrows represent the lateral extension of the mountain range as it collapses under its own weight. Note the associated thinning of the lithosphere (in grey) beneath the orogen.

Post-orogenic decompression melting is the result of a reduction in pressure as a newly formed mountain range extends due to its own weight and the relaxation in tectonic compressional forces. The reduced pressure lowers the liquidus enabling the underlying rock to melt. Figure 20 is an illustration of this process (after Winters, 2014).

Limitations

From the above Discussion it is permitted to suggest that the Granitoids and the KZ are compositionally linked. Limitations to this conclusion relate to the number of Granitoid samples, which in this study is minimal and may not be statistically representative. The data for the KZ are only average compositions of the two sections, which may obscure compositional relationships.

While discrimination diagrams were selected based on a high percentage of correct classifications, it should be noted that discrimination diagrams are more suggestive than defining. In the case of the Granitoids it was shown how samples may be shifted into other fields. It can be difficult to define the tectonic setting of granitic rocks, as discussed in Rollinson & Pease (2021). Granitic melt chemical compositions can be altered by either crystal fractionations or hydrothermal fluids. These processes may affect the geochemical signature of the granite, leading to misclassifications.

PER diagrams have limitations as discussed by Rollinson & Pease (2021). It has been shown that a PER diagram can give misleading interpretations. Another approach is to use multiple conserved elements as described by Nicholls and Russell (2016) which is an avenue for future investigations.

During data interpretation, assumptions must be made. A key assumption in the Discussion is the relationship within the KZ of the Granulites to the Amphibolites to be able to extrapolate a relationship to the Granitoids. It should be noted that this study is not definitive; suggestions have been put forward about the origins of the MC and Granitoids in respect to the KZ, along with the reasoning behind them.

Future studies

Isotopic geochemical data is lacking from this study but would significantly improve the ability to understand these rocks as it could be used to suggest mantle reservoirs, as well as mixing scenarios and tectonic environments. It would be an enlightening avenue and help to understand the genesis of the MC and its relationship to the surrounding rocks.

Conclusions

This study suggests that:

- The MC originated at depths of greater than 80 km (HREE signature of garnet, the presence of spinel and pigeonite exsolution).
- The MC magma has a source influenced by subduction processes (decoupling of the LILE from the HFSE).
- The MC evolved from crystal fractionation processes (plagioclase and/or olivine with a rejuvenation event).
- No compositional relationship was found between the MC and the KZ and Granitoids.
- The Granitoids represent a partial melt extracted from the KZ (compositional link between the Granitoids and the KZ and similar REE patterns).
- The tectonic environment for the Granitoids is presumed to reflect decompression melting (due to lateral spreading during post-orogenic collapse).

Acknowledgements

I would like to acknowledge the support from my peers, my partner, and my professor. This thesis would not be at the quality it is without them. Thank you.

Bibliography

Le Bas, M., & Streckeisen, A. 1991. *The IUGS systematics of igneous rocks,* Journal of the Geological Society, London, Vol. pp. 148, 825-833.

Nicholls, J., & Russell, J.K., 2016. *Igneous rock associations 20. Pearce element ratio diagrams: Linking geochemical data to magmatic processes.* Geoscience Canada 43, 133–146.

Pearce, J.A., Harris, N.B., & Tindle, A.G., 1984. *Trace element discrimination diagrams for the tectonic interpretation of granitic rocks.* Journal of Petrology 25, 956–983.

Pearce, T.H., 1968. *A contribution to the theory of variation diagrams.* Contributions to Mineralogy and Petrology 19, 142–157.

Peressini, G., Quick, J.E., Sinigoi, S., Hofmann, A.W., & Fanning, M., 2007. *Duration of a Large Mafic Intrusion and Heat Transfer in the Lower Crust: a SHRIMP U/Pb Zircon Study in the IVZ (Western Alps, Italy).* Journal of Petrology 48, pp. 1185-1218.

Philpotts, A. R. 2003. *Petrography of Igneous and Metamorphic Rocks*, Waveland Press, Prospect Heights, IL.

Pinarelli, L., Del Moro, A., & Boriani, A., 1988. *Rb–Sr geochronology of lower Permian plutonosm in Massiccio dei Laghi, Southern Alps (NW Italy).* Rendiconti della Societa Italiana di Mineralogia e Petrologia 43, pp. 411–428.

Pinarelli, L., Del Moro, A., Boriani, A., & Caironi, V., 2002, *Sr, Nd isotope evidence for an enriched mantle component in the origins of the Hercynian gabbro -granite series of the "Serie dei Laghi" (Southern Alps, northwestern Italy), European Journal of Mineralogy*, vol. 14, no. 2, pp. 403–415

Quick, J. E., Sinigoi, S., Snoke, A. W., Kalakay, T. J., Mayer, A., & Peressini, G., 2002. *Geologic map of the southern Ivrea-Verbano zone, northwestern Italy.* USGS https://doi.org/10.3133/i2776

Rivalenti, G., Garuti, G., & Rossi, A., 1975. *The origin of the Ivrea- Verbano basic formation (western Italian Alps): Whole rock geochemistry.* Bollettino della Società Geologica Italiana 94, 1149-1186.

Rivalenti, G., Garutti, G., Rossi, A., Siena, F., & Sinigoi, S., 1980. *Existence of different peridotite types and of a layered igneous complex in the Ivrea zone of the Western Alps.* Journal of Petrology 22: pp. 127-153.

Rivalenti, G., Rossi, A., Siena, F., & Sinigoi, S., 1984. *The layered series of the Ivrea-Verbano Igneous Complex, Western Alps, Italy.* Tschermaks Mineralogische Petrographische Mitteilungen, 33: 77-99.

Rollinson, H., & Pease, V., 2021. *Using Geochemical Data to Understand Geological Processes Second Edition.* Cambridge University Press

Schnetger, B., 1994. *Partial melting during the evolution of the amphibolite- to granulite-facies gneisses of the Ivrea Zone, northern Italy*, Chemical Geology, Volume 113, Issues 1–2, pp. 71-101, https://doi.org/10.1016/0009-2541(94)90006-X.

Sinigoi, S., Quick, J., Clemens-Knott, D., Mayer, A. Demarchi, G., Mazzucchelli, M., Negrini, L., & Rivalenti, G., (1994), *Chemical evolution of a large mafic intrusion in the lower crust, Ivrea-Verbano Zone, northern Italy*, J. Geophys. Res., 99(B11), 21575–21590, doi:10.1029/94JB00114.

Sun, S.S., & McDonough, W.F., 1989. *Chemical and isotopic systematics of oceanic basalts: Implications for mantle composition and processes,* Magmatism in ocean basins, Geological Society Special Publication 42. Geological Society, London. Pp. 313–345.

Verma, S.P., Pandarinath, K., Verma, S.K., & Agrawal, S., 2013. *Fifteen new discriminant-function-based multi-dimensional robust diagrams for acid rocks and their application to Precambrian rocks.* Lithos 168–169, 113–123.

Vermeesch, P., 2006a. *Tectonic discrimination diagrams revisited.* Geochemistry, Geophysics, Geosystems 7, Q06017, doi: 10.1029/2005GC001092.

Winters, J. D., 2014, *Principles of Igneous and Metamorphic Petrology,* Pearson Education Limited.

Appendix A

BA 1905 – 1

Hand sample description:

Colour:	Grain size:	Texture:	Visible minerals:	Rock type:
Bulk rock: Dark green Vein: Stronger lighter green Crust: Beige	Phaneritic 0.2-1 mm	Equigranular	Pyroxene Olivine	Intrusive

Thin section description:

MINERALOGY Modal % → Normalized %	PPL	XPL
Clinopyroxene 49% → 49%	High relief	Second order colours
Orthopyroxene 33% → 33%	High relief Green	First order colours Twinning
Olivine 18% → 18%	High relief Irregular fractures	Third order colours
Spinel <1%	Anhedral High relief Strong brown colour	Isotropic

Crystallization sequence: Spinel, Olivine, Orthopyroxene ~ Clinopyroxene

IUGS rock name:

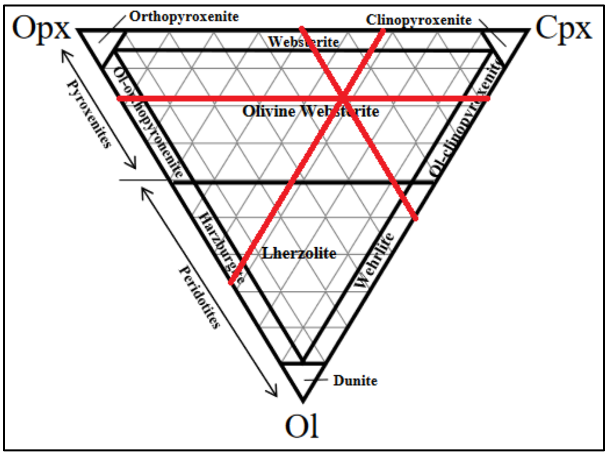

Olivine Websterite

Thin section scans:

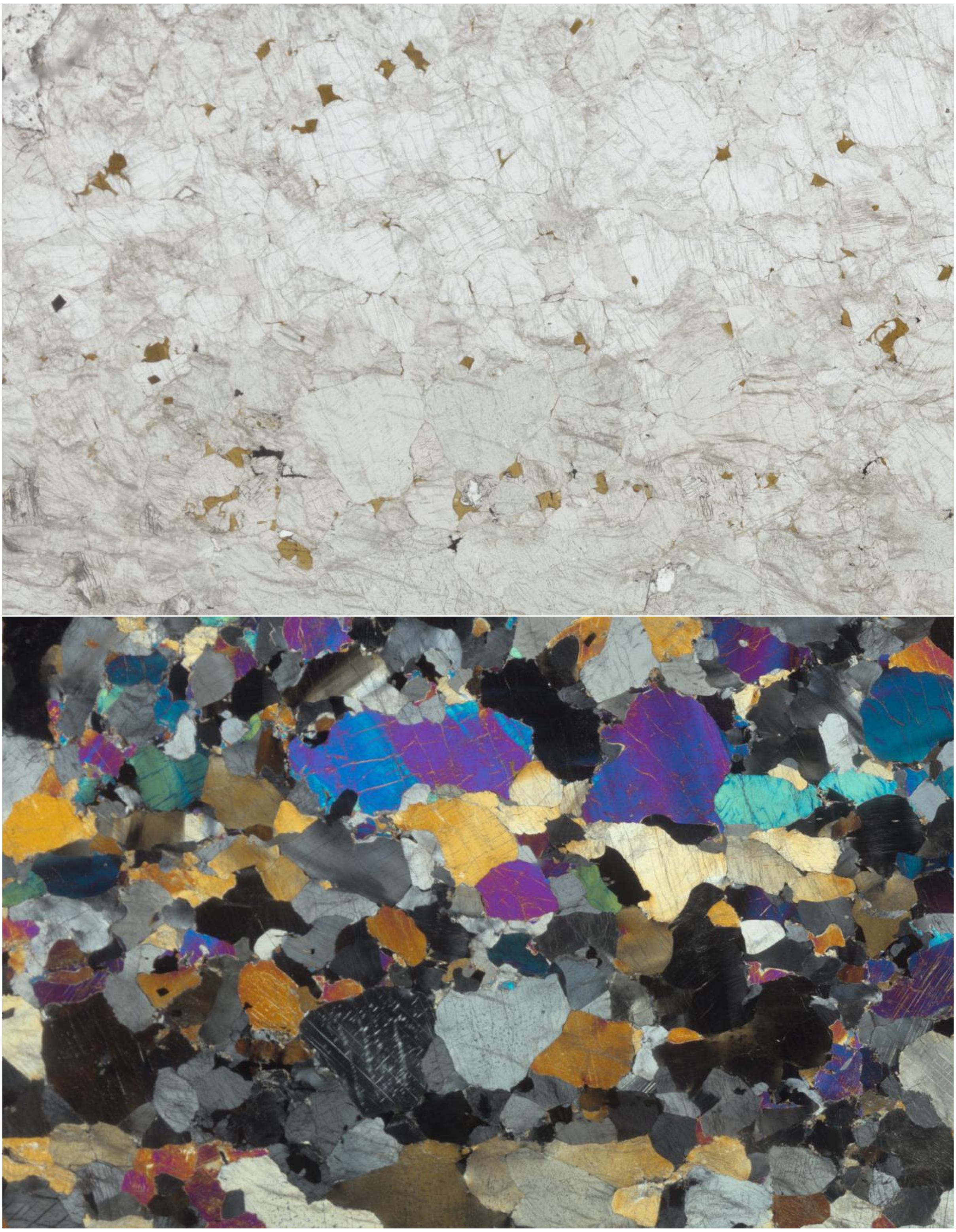

Figure A1. Cropped thin section scan in both PPL (Top) and XPL (Bottom). Field of view is approximately 1.8 mm.

BA 2335 – B

Hand sample description:

Colour:	Grain size:	Texture:	Visible minerals:	Rock type:
Crust: Beige with streaks Fresh cut: Green	0.2-1 mm	Cumulate	Pyroxenes Olivine Spinel	Intrusive

Thin section description:

MINERALOGY Modal % → Normalized %	PPL	XPL
Orthopyroxene 31.7% → 37.3%	High relief Pink	First order colours
Clinopyroxene 30.8% → 36.2%	High relief	Second order colours
Olivine 22.5% → 26.5%	High relief Irregular fractures	Third order colours
Spinel 15%	Anhedral High relief Green	Isotropic

Crystallization sequence: Spinel, Olivine, Orthopyroxene ~ Clinopyroxene

IUGS rock name:

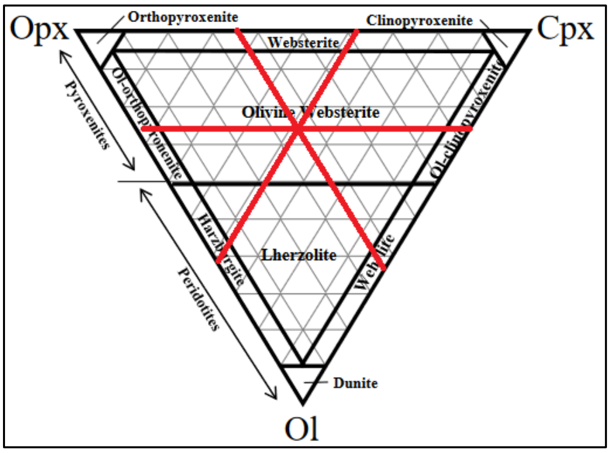

Olivine Websterite

Thin section scans:

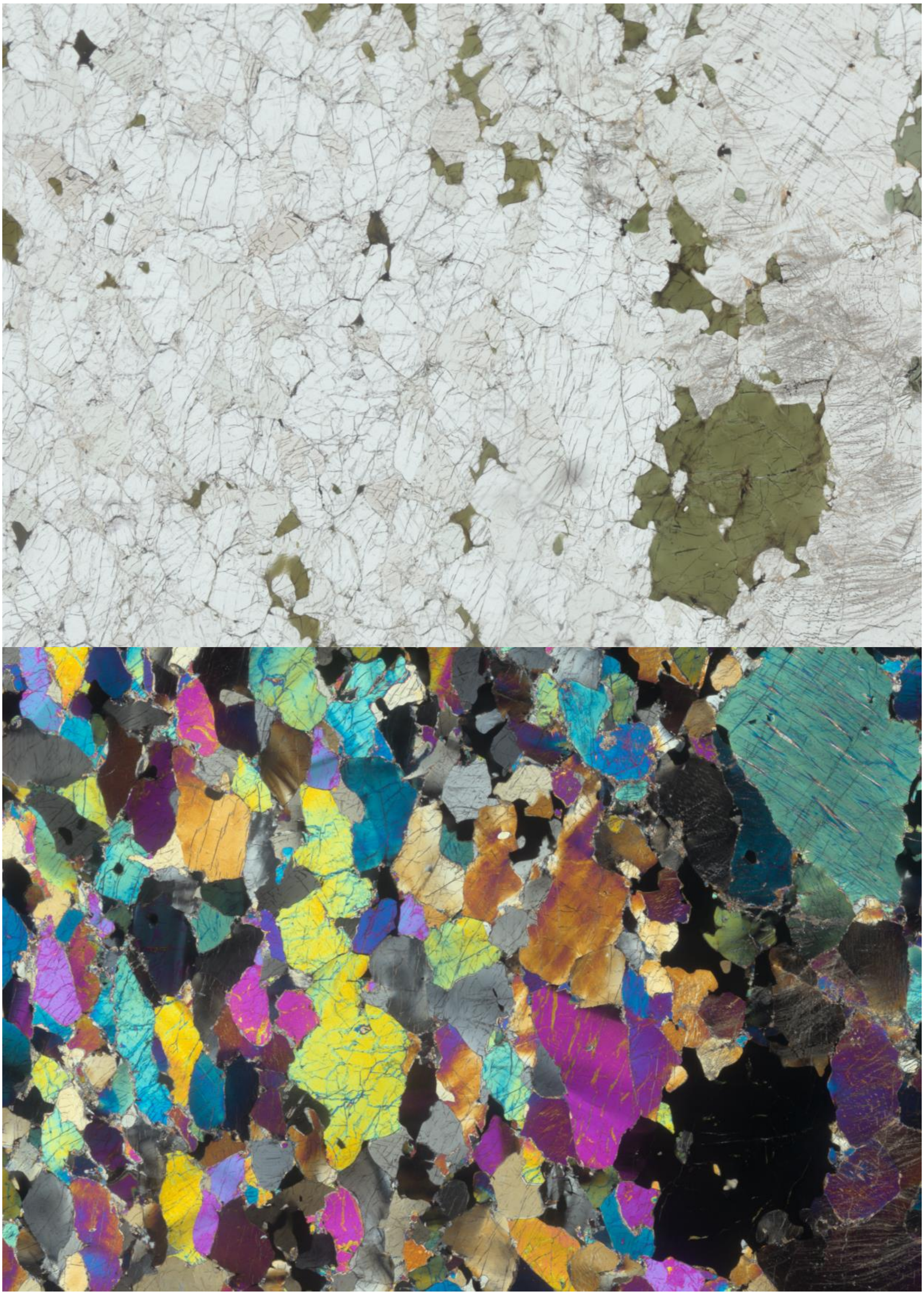

Figure A2. Cropped thin section scan in both PPL (Top) and XPL (Bottom). Field of view is approximately 1.4 mm mm.

IV 1906 – 1

Hand sample description:

Colour:	Grain size:	Texture:	Visible minerals:	Rock type:
Melanocratic	Phaneritic 1 - 5 mm	Inequigranular	Plagioclase Pyroxenes Olivine	Intrusive

Thin section description:

MINERALOGY Modal % → Normalized %	PPL	XPL
Plagioclase 44% → 50%	Low relief	First order colours Polysynthetic twinning
Clinopyroxene 27% → 44%	High relief	Second order colours Simple twinning
Orthopyroxene 11% → 44%	High relief	First order colours
Amphibole 9%	Brown pleochroism Anhedral	Second order
Olivine 5% → 6%	High relief Irregular fractures	Third order colours
Spinel 4%	Anhedral Dark green to opaque	Isotropic

Crystallization sequence: Olivine, Spinel, Pyroxene, Plagioclase ~ Amphibole

IUGS rock name:

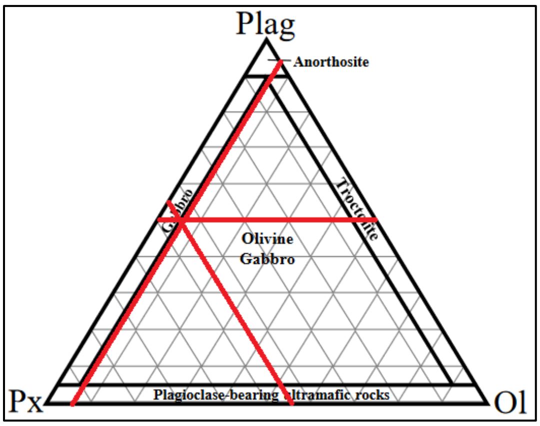

Olivine Gabbro

Thin section scans:

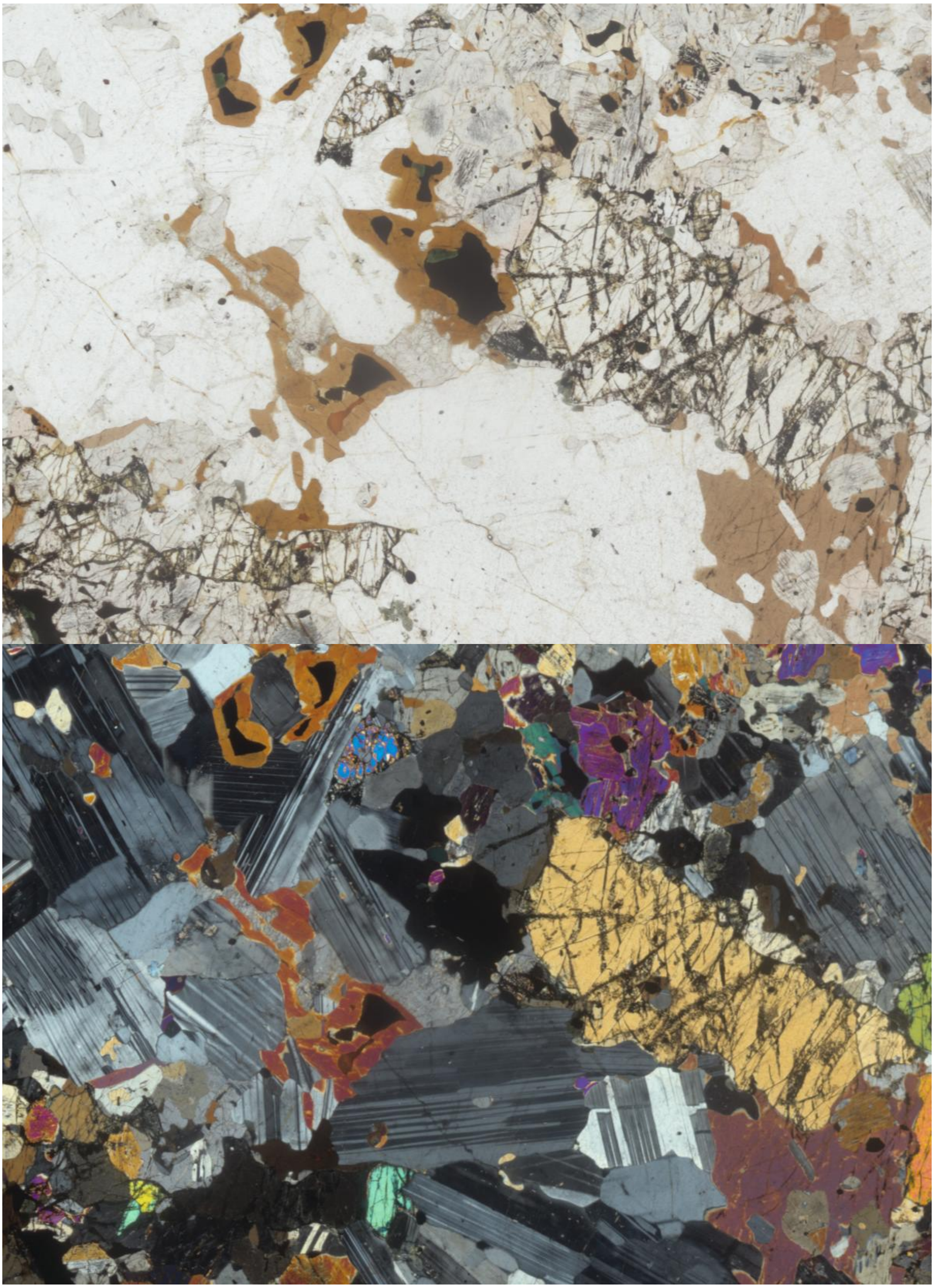

Figure A3. Cropped thin section scan in both PPL (Top) and XPL (Bottom). Field of view is approximately 0.8 mm.

IV 1907 – 1

Hand sample description:

Colour:	Grain size:	Texture:	Visible minerals:	Rock type:
Pink	Very fine <0.2 mm	Layered	Quartz	Extrusive

Thin section description:

MINERALOGY Modal % → Normalized %	PPL	XPL
Quartz	Colourless Anhedral	Anisotropic
Plagioclase	Subhedral	Twinning

Notes: Devitrified glass texture with quartz and plagioclase phenocrysts.

IUGS rock name:

Tuff – Rhyolite

Thin section scans:

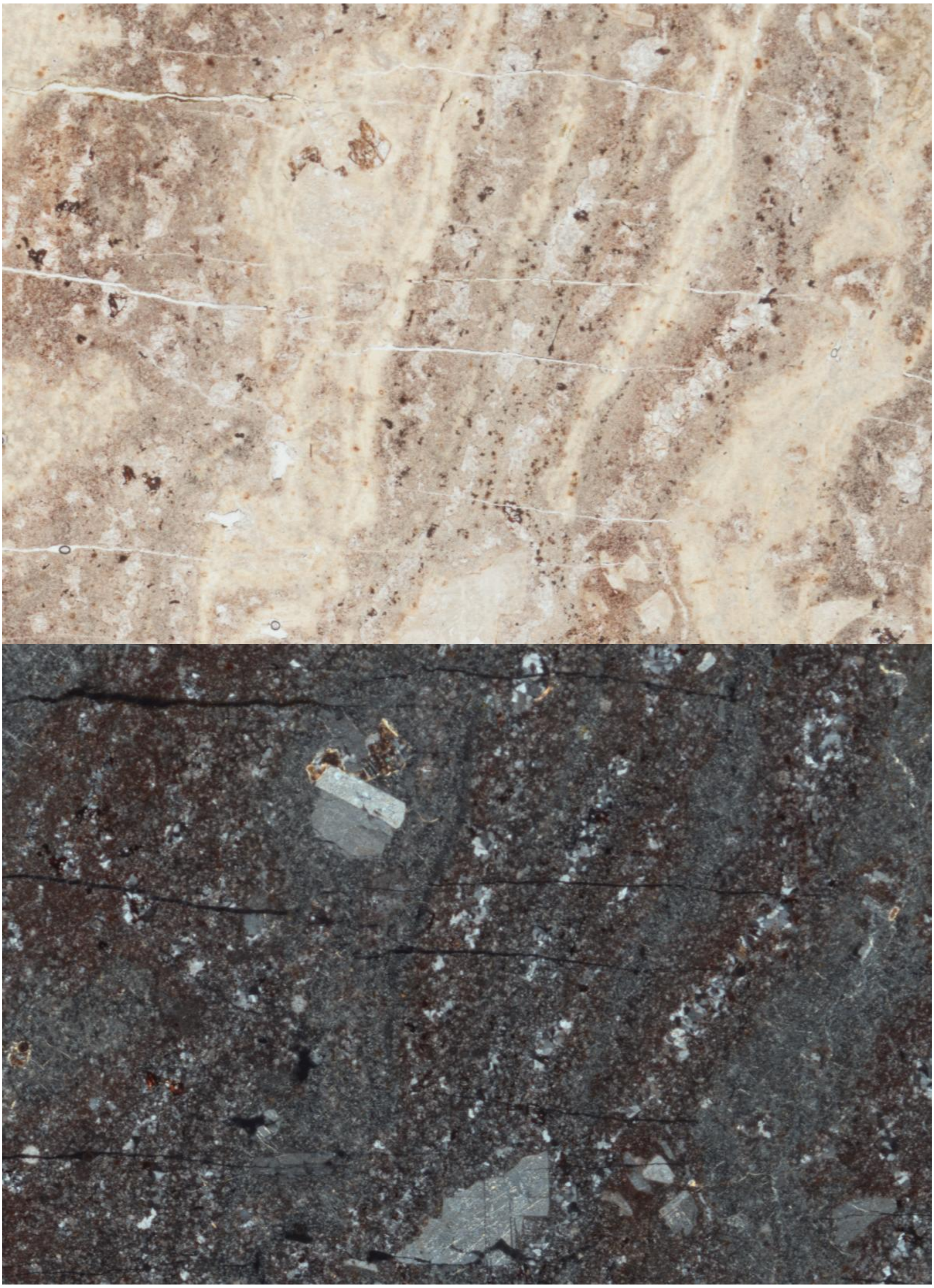

Figure A4. Cropped thin section scan in both PPL (Top) and XPL (Bottom). Field of view is approximately 0.8 mm.

IV 2336 – B

Hand sample description:

Colour:	Grain size:	Texture:	Visible minerals:	Rock type:
Melanocratic	0.2-1mm	Equigranular	Pyroxene Plagioclase Lizardite	Intrusive

Thin section description:

MINERALOGY Modal % → Normalized %	PPL	XPL
Plagioclase 52% → 55%	Low relief	First order colour Polysynthetic twinning
Olivine 25% → 26%	High relief Irregular fractures	Third order colours Serpentinization
Clinopyroxene 18% → 19%	Very high relief	Second order colours
Lizardite 5%	Yellow Fibrous	Analogous Blue/grey

Crystallization sequence: Clinopyroxene, Olivine, Plagioclase, Serpentine

IUGS rock name:

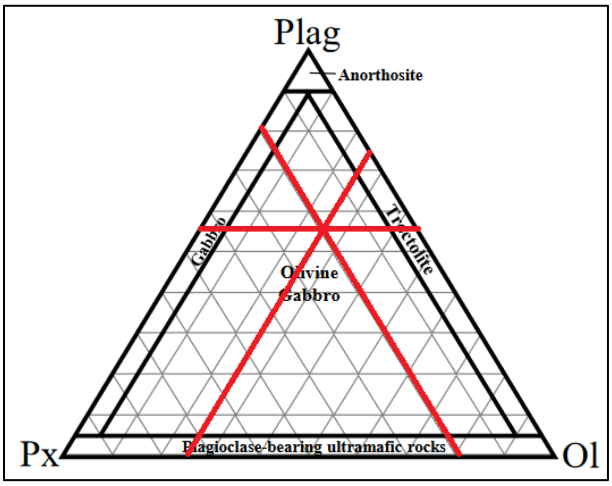

Olivine Gabbro

Thin section scans:

Figure A5. Cropped thin section scan in both PPL (Top) and XPL (Bottom). Field of view is approximately 0.8 mm.

IV 2337 – A

Hand sample description:

Colour:	Grain size:	Texture:	Visible minerals:	Rock type:
Dark blue	0.2-1mm	Granoblastic	Pyroxene	Intrusive

Thin section description:

MINERALOGY Modal % → Normalized %	PPL	XPL
Orthopyroxene 66% → 78%	High relief Pink pleochroism	First-low second order colours
Clinopyroxene 16.2% → 19%	High relief	Second-low third order colours
Amphibole 7.8%	Brown pleochroism	Low third order
Spinel 7.5%	Anhedral High relief Dark green / Opaque	Isotropic
Olivine 2.5% → 3%	High relief Blue pleochroism	High third order colours

Crystallization sequence: Spinel, Olivine, Clinopyroxene ~ Orthopyroxene, Amphibole

IUGS rock name:

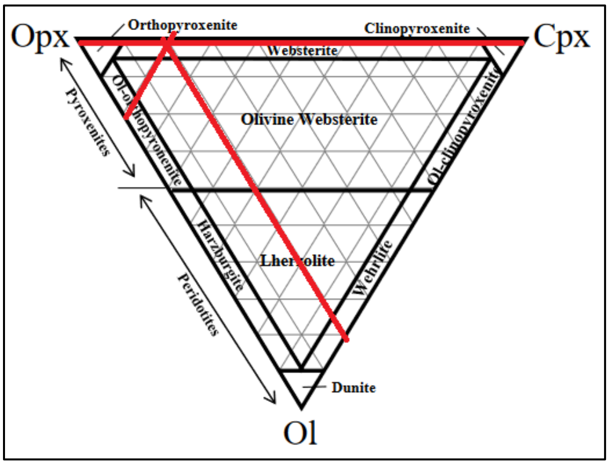

Websterite

Thin section scans:

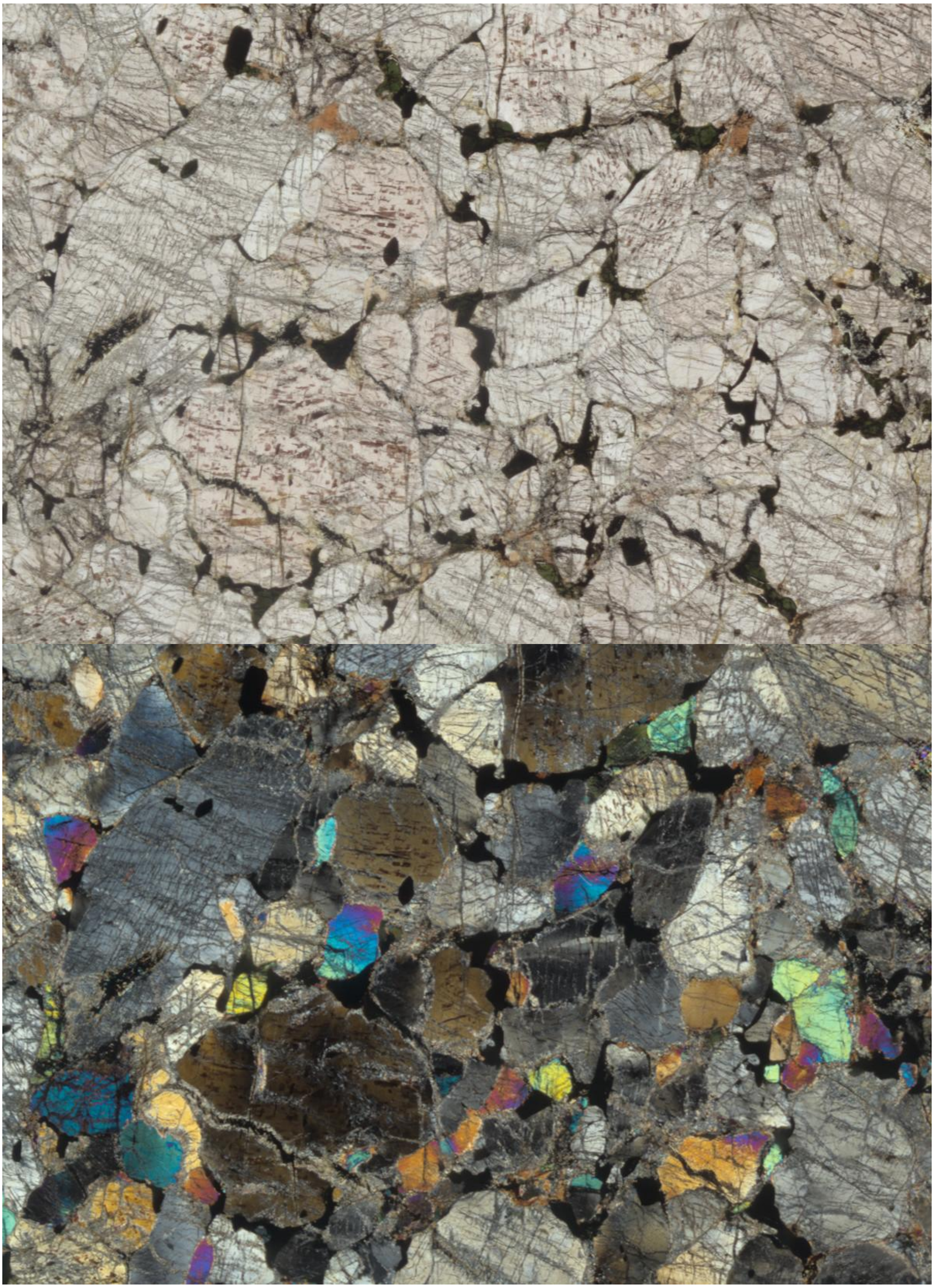

Figure A6. Cropped thin section scan in both PPL (Top) and XPL (Bottom). Field of view is approximately 0.8 mm. The thin section is a little thick therefore the colours are slightly higher.

IV 2340 – B

Hand sample description:

Colour:	Grain size:	Texture:	Visible minerals:	Rock type:
White Green	1-5 mm	Inequigranular	Feldspar Quartz Chlorite Garnet Biotite	Intrusive

Thin section description:

MINERALOGY Modal % → Normalized %	PPL	XPL
Alkali-Feldspar 48.1% → 59.2%	Medium relief Exsolution lines	Low colours
Quartz 33.1% → 40.8%	Low relief	White Patchy extinction
Chlorite 6.9%	Green High relief	Analogous Fibrous
Garnet 6.3%	High relief Fractured Subhedral	Isotropic
Biotite 5.6%	Brown pleochroism Sheeted	Third order colours

Crystallization sequence: Biotite, Garnet, Feldspar, quartz, chlorite

IUGS rock name:

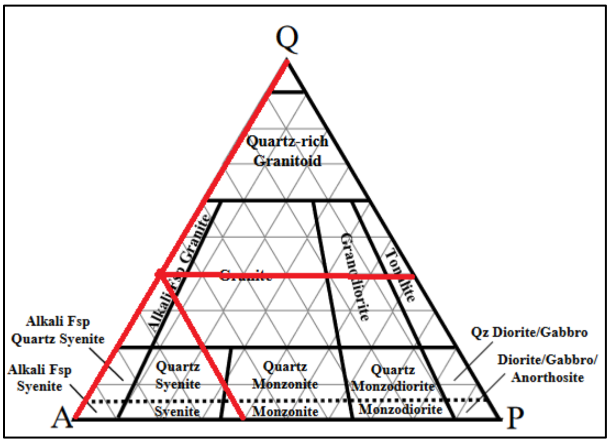

Alkali-Feldspar Granite

Thin section scans:

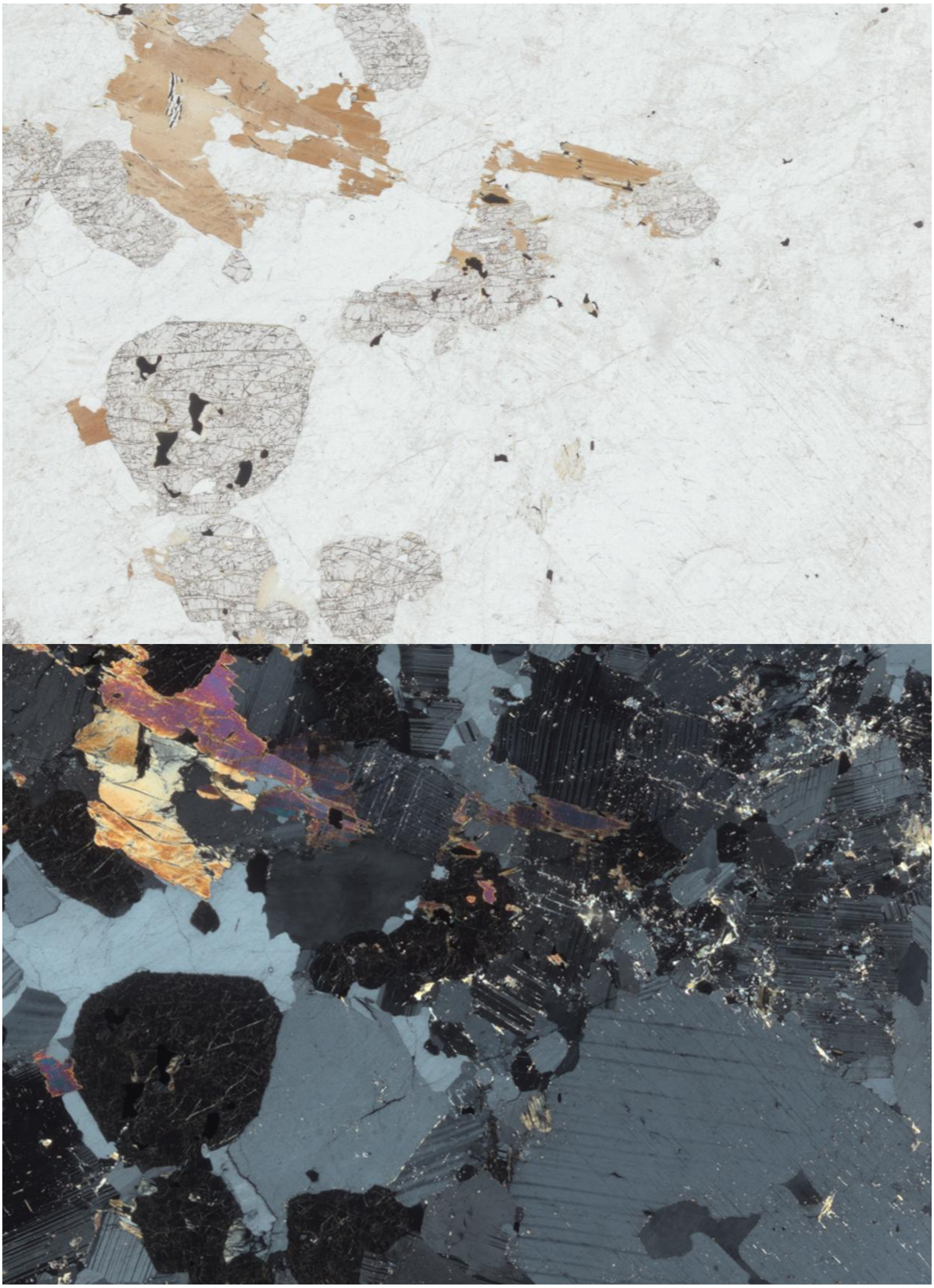

Figure A7. Cropped thin section scan in both PPL (Top) and XPL (Bottom). Field of view is approximately 0.8 mm.

IV 2341 – C

Hand sample description:

Colour:	Grain size:	Texture:	Visible minerals:	Rock type:
White	Inequigranular 0.2-1 mm	Aplitic	Quartz Feldspar Biotite Muscovite	Intrusive

Thin section description:

MINERALOGY Modal % → Normalized %	PPL	XPL
Quartz 45.5% → 50%	Low relief	Patchy extinction White
Plagioclase 32.5% → 35.7%	Low relief	Polysynthetic twinning Saussuritized cores
Alkali-feldspar 13% → 14.3%	Low relief	Tartan twinning
Muscovite 8%	Moderate relief Shard-like crystal habit Tabular cleavage	Second to third order colours Flat grains have first order colours and simple twinning
Biotite 1%	Brown pleochroism Tabular cleavage	Second order colours

Crystallization sequence: Plagioclase, Biotite ~ Muscovite, Quartz, Alkali Feldspar

IUGS rock name:

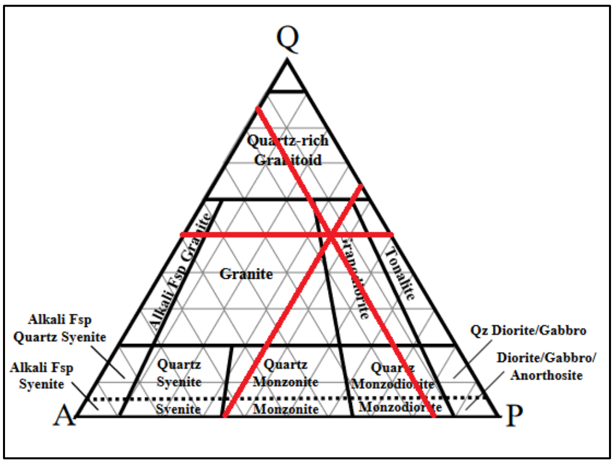

Granodiorite

Thin section scans:

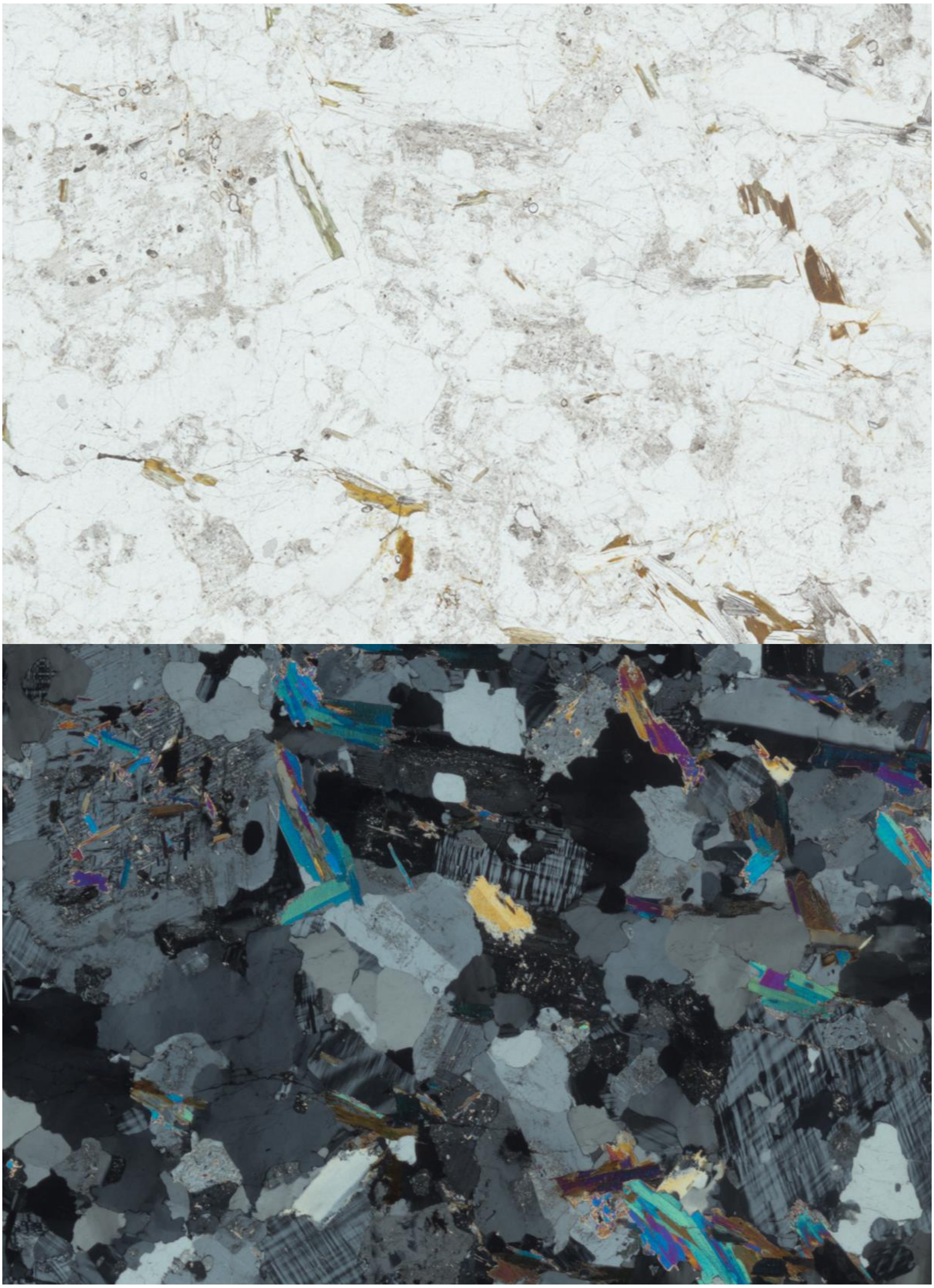

Figure A8. Cropped thin section scan in both PPL (Top) and XPL (Bottom). Field of view is approximately 0.8 mm.

IV 2343 – A

Hand sample description:

Colour:	Grain size:	Texture:	Visible minerals:	Rock type:
White	1-5 mm	Inequigranular	Biotite Quartz Feldspar	Intrusive

Thin section description:

MINERALOGY Modal % → Normalized %	PPL	XPL
Plagioclase 40.4% → 44.2%	low relief	Polysynthetic twinning Saussuritized cores
Quartz 30.8% → 33.7%	Low relief	White Patchy extinction
Alkali-Feldspar 20.2% → 22.1%	Low relief Exsolution lines	Tartan twinning Low first order colour
Biotite 8.6%	Strong brown pleochroism Tabular cleavage	Second order colour Straight extinction
Chlorite <1%	Green	Analogous
Muscovite <1%	Colourless needle filling gaps within biotite	Low third order colours
Zircon <1%	Colourless High relief	High second order colours Reaction halos

Crystallization sequence: Zircon, Plagioclase, Biotite, Quartz, Alkali-Feldspar, Muscovite, Chlorite

IUGS rock name:

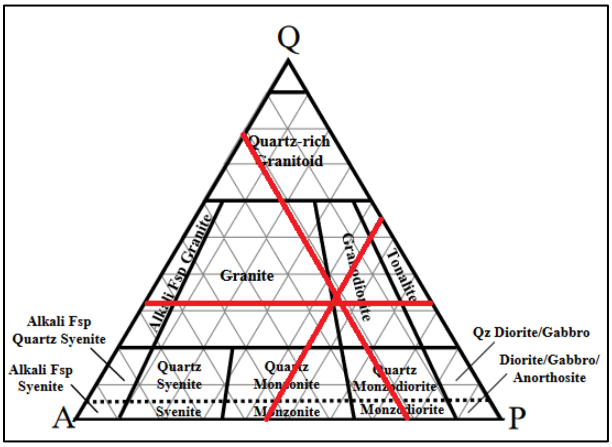

Granodiorite

Thin section scans:

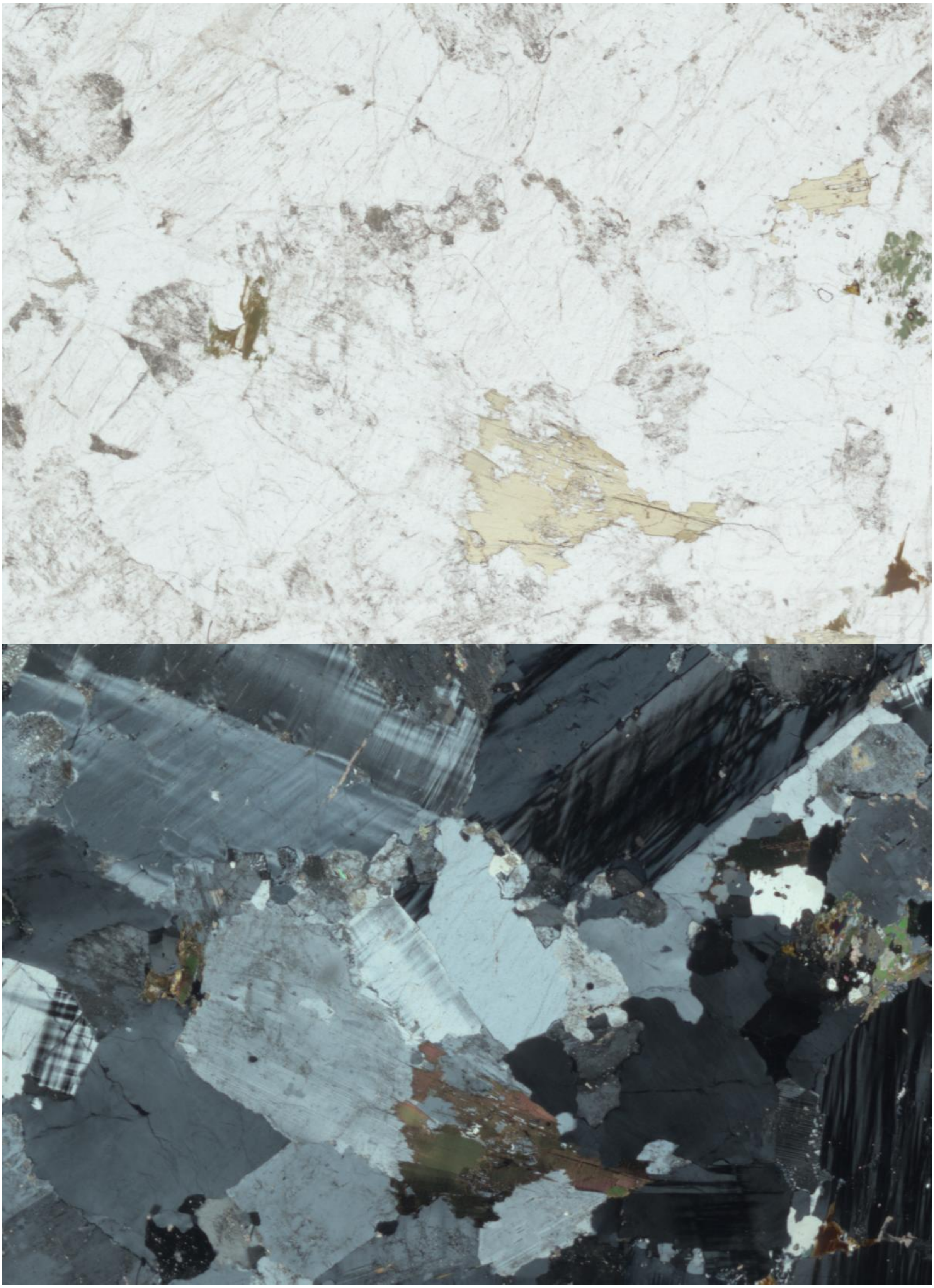

Figure A9. Cropped thin section scan in both PPL (Top) and XPL (Bottom). Field of view is approximately 0.8 mm.

SL 1909 – 3

Hand sample description:

Colour:	Grain size:	Texture:	Visible minerals:	Rock type:
White	1-5 mm	Inequigranular	Quartz Biotite Feldspar	Intrusive

Thin section description:

MINERALOGY Modal % → Normalized %	PPL	XPL
Quartz 36.8% → 37.7%	Colourless Low relief	Patchy extinction White
Alkali Feldspar 33.1% → 33.9%	Medium relief Exsolution lineation	First order colours
Plagioclase 27.6% → 28.4%	Low relief	Polysynthetic Twinning Saussuritized cores
Zircon <0.1%	Clear subhedral crystals	Third order colours Reaction halos
Chlorite <0.1%	Green pleochroism	Analogous

Crystallization sequence: Zircon, Plagioclase, Biotite, Alkali Feldspar ~ Quartz, Chlorite

IUGS rock name:

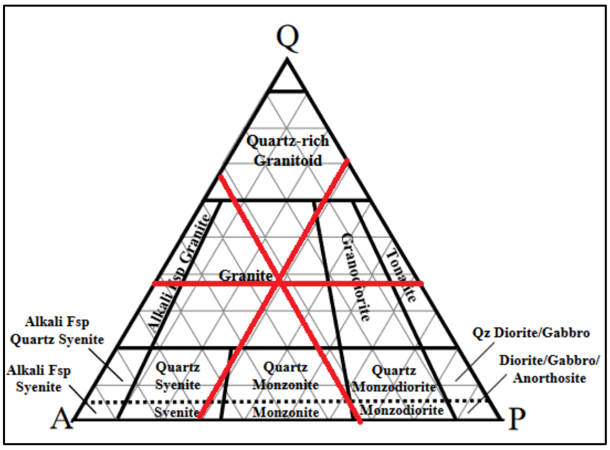

Granite

Thin section scans:

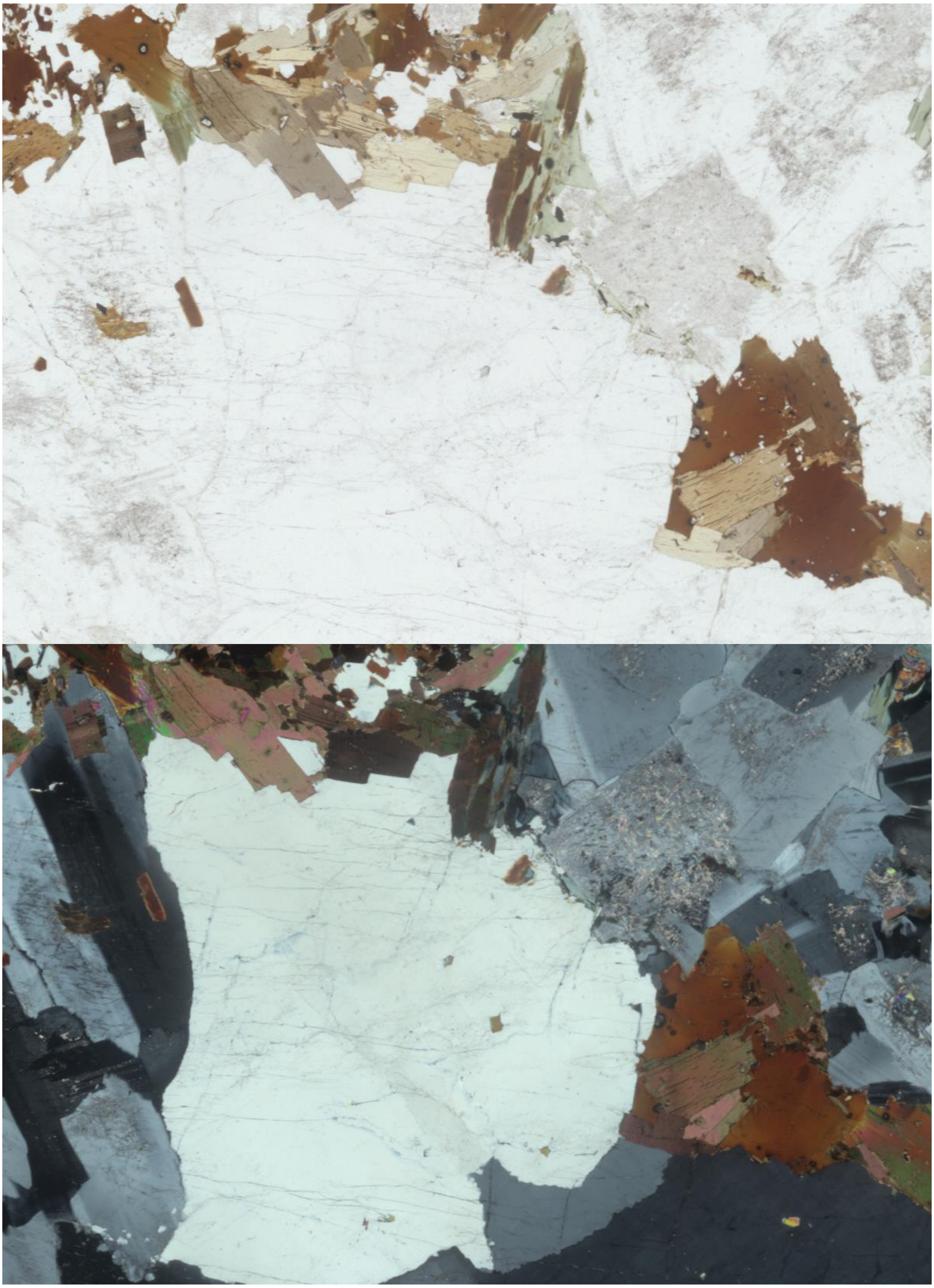

Figure A10. Cropped thin section scan in both PPL (Top) and XPL (Bottom). Field of view is approximately 0.8 mm. Zircons, and their radiation halos are visible in the biotite sheets.

Appendix B

Mafic Complex data table

Table B1						
Sample ID	BZ 1	BZ 2	BZ 3	BZ 4	MZ 1	MZ 2
TAS name	Foid Gabbro	Alkalic Gabbro	Alkalic Gabbro	Subalkalic Gabbro	Peridot Gabbro	Peridot Gabbro
Rock Unit	Basal zone	Basal zone	Basal zone	Basal zone	Main zone	Main zone
Source	Rivalenti	Rivalenti	Rivalenti	Rivalenti	Sinigoi	Sinigoi
Method	ARL-EM	ARL-EM	ARL-EM	ARL-EM	XRF & ICPMS	XRF & ICPMS
MAJOR ELEMENTS (WT %)						
SiO_2	43.10	44.30	45.34	46.70	44.86	44.89
TiO_2	2.93	2.75	2.08	1.51	1.71	0.27
Al_2O_3	20.50	15.7	18.45	14.00	20.30	20.54
FeO^{TOT}	10.10	14.06	12.68	10.98	12.08	9.09
MnO	0.14	0.26	0.21	0.22	0.17	0.15
MgO	4.85	7.1	6.48	11.24	8.64	12.67
CaO	11.42	11.67	12.18	13.75	8.91	10.98
Na_2O	3.06	2.42	1.96	1.50	2.40	1.26
K_2O	0.38	0.04	0.49	0.06	0.18	0.13
P_2O_5	1.80	0.08	0.14	0.02	0.74	0.01
Total	98.28	98.38	100.00	99.98	100.00	100.00
TRACE ELEMENTS (PPM)						
Rb	2.66	0.12	2.5	0.37	1.30	1.10
Sr	585.00	101.00	442.00	210.00	567.50	445.70
Y	16.00	55.00	14.00	38.00	7.20	4.00
Zr	141.00	107.00	150.40	73.00	15.30	24.00
Nb	9.00	4.00	2.30	3.00	1.50	0.40
Ba	832.00	1.00	320.00	2.50	216.00	109.00
La	21.06	1.01	13.20	1.20	9.40	3.00
Ce	50.54	6.66	29.50	6.40	20.30	5.90
Pr	7.08	1.47	4.17	1.33	2.80	0.82
Nd	27.43	10.2	19.40	8.20	12.40	3.30
Sm	6.12	4.47	3.90	3.30	2.41	0.83
Eu	4.06	1.62	2.12	1.27	2.46	0.72
Gd	5.71	7.07	3.51	5.12	2.31	0.85
Tb	0.63	1.24	0.52	0.89	0.28	0.13
Dy	-	-	2.81	-	1.67	0.77
Ho	0.62	1.79	0.58	1.20	0.26	0.16
Er	1.62	5.62	1.69	3.80	0.58	0.42
Tm	0.20	0.82	0.22	0.55	0.10	0.06
Yb	1.14	5.17	1.41	3.38	0.41	0.30
Lu	0.17	0.76	0.23	0.47	0.06	0.08
Hf	-	-	3.80	-	0.20	0.50
Ta	-	-	0.20	-	0.20	0.10
Th	-	-	0.20	-	0.20	0.20
U	-	-	0.10	-	0.10	0.10

Table B1 Continued						
Sample ID	MZ 3	MZ 4	UZ 1	UZ 2	UZ 3	UZ 4
TAS name	Alkalic Gabbro	Subalkalic Gabbro	Alkalic Gabbro	Subalkalic Gabbro	Subalkalic Gabbro	Monzonite
Rock Unit	Main Zone	Main Zone	Upper Zone	Upper Zone	Upper Zone	Upper Zone
Source	Sinigoi	Sinigoi	Sinigoi	Sinigoi	Sinigoi	Sinigoi
Method	XRF & ICPMS	XRF & ICPMS	XRF & SSMS	XRF & ICPMS	XRF & SSMS	XRF & ICPMS
MAJOR ELEMENTS (WT %)						
SiO_2	46.99	47.14	47.74	48.10	49.28	54.50
TiO_2	2.16	0.92	2.23	0.32	0.54	1.29
Al_2O_3	23.53	20.59	20.45	26.20	19.38	19.00
FeO^{TOT}	7.49	10.66	9.40	5.69	10.22	7.75
MnO	0.09	0.20	0.14	0.20	0.18	0.15
MgO	5.76	7.47	5.52	4.32	7.00	2.91
CaO	10.98	10.95	11.14	12.17	11.21	5.46
Na_2O	2.59	1.90	2.78	2.10	1.95	3.36
K_2O	0.38	0.14	0.57	0.20	0.21	4.58
P_2O_5	0.03	0.02	0.03	0.06	0.03	0.07
Total	100.00	100.00	100.00	99.36	100.00	99.07
TRACE ELEMENTS (PPM)						
Rb	3.10	2.30	1.70	1.29	0.50	55.00
Sr	606.60	417.00	660.20	596.00	499.50	434.00
Y	5.40	7.00	12.50	2.00	5.60	8.18
Zr	76.50	18.30	114.00	36.00	22.40	1745.00
Nb	2.80	0.40	4.00	5.00	0.40	9.00
Ba	276.00	114.00	557.00	571.00	322.00	3344.00
La	7.00	2.90	17.40	5.36	4.10	18.75
Ce	13.50	6.30	35.00	11.86	8.60	25.27
Pr	1.84	0.95	4.80	1.35	1.12	-
Nd	7.80	5.40	21.60	5.57	5.30	10.07
Sm	1.45	1.24	3.88	0.86	1.12	1.85
Eu	1.20	1.58	3.05	2.56	1.58	5.70
Gd	1.21	1.34	3.52	0.79	1.29	1.44
Tb	0.20	0.21	0.48	0.11	0.19	0.51
Dy	0.95	1.19	2.88	-	1.09	1.26
Ho	0.20	0.28	0.52	0.15	0.24	0.68
Er	0.60	0.72	1.46	0.44	0.63	0.88
Tm	0.09	0.12	0.16	0.07	0.09	-
Yb	0.48	0.68	1.04	0.54	0.61	1.37
Lu	0.10	0.11	0.16	-	0.09	0.25
Hf	1.40	0.60	2.60	-	0.70	-
Ta	0.30	0.10	0.30	-	0.10	-
Th	0.20	0.20	0.20	-	0.20	-
U	0.10	0.10	0.10	-	0.10	-

Table B1 Continued					
Sample ID	UZ 5	EUMC 1	EUMC 2	EUMC 3	EUMC 4
TAS name	Monzonite	Peridot Gabbro	Alkalic Gabbro	Alkalic Gabbro	Alkalic Gabbro
Rock Unit	Upper Zone	Enclaves in Diorite from the Upper MC	Enclaves in Diorite from the Upper MC	Enclaves in Diorite from the Upper MC	Enclaves in Diorite from the Upper MC
Source	Sinigoi	Sinigoi	Sinigoi	Sinigoi	Sinigoi
Method	XRF & ICPMS	XRF & SSMS	XRF & SSMS	XRF & SSMS	XRF & SSMS
MAJOR ELEMENTS (WT %)					
SiO_2	55.20	44.89	45.92	46.66	46.79
TiO_2	1.16	2.16	1.84	1.56	1.53
Al_2O_3	18.30	16.61	17.84	17.80	17.85
FeO^{TOT}	8.38	12.20	11.17	10.97	11.08
MnO	0.20	0.20	0.19	0.21	0.22
MgO	1.65	8.73	8.33	8.45	8.52
CaO	5.32	11.83	11.76	11.30	11.45
Na_2O	2.60	1.83	1.81	1.99	1.74
K_2O	5.97	1.05	1.10	1.01	0.80
P_2O_5	0.79	0.49	0.04	0.05	0.03
Total	99.57	100.00	100.00	100.00	100.00
TRACE ELEMENTS (PPM)					
Rb	43.00	12.40	10.00	10.50	4.80
Sr	352.00	519.60	432.40	405.90	413.40
Y	21.00	27.80	44.90	37.00	40.30
Zr	1341.00	161.10	209.80	236.90	205.30
Nb	7.00	8.70	10.30	8.10	8.50
Ba	6956.00	494.00	405.00	431.00	270.00
La	36.70	25.10	22.60	19.20	20.00
Ce	73.20	68.00	66.00	52.90	56.90
Pr	-	10.36	10.63	8.59	9.30
Nd	35.90	48.50	54.10	43.90	46.90
Sm	5.43	8.93	11.81	9.43	10.41
Eu	6.83	2.89	3.95	3.43	3.62
Gd	-	7.18	10.57	8.72	9.48
Tb	-	1.05	1.66	1.35	1.48
Dy	-	5.80	9.24	7.42	8.10
Ho	-	1.03	1.69	1.43	1.50
Er	-	2.74	4.69	3.82	4.17
Tm	-	0.42	0.68	0.56	0.59
Yb	1.91	2.33	3.83	3.15	3.48
Lu	0.34	0.34	0.56	0.48	0.51
Hf	-	4.70	6.00	6.00	5.90
Ta	-	0.70	0.70	0.60	0.70
Th	-	0.30	0.40	0.20	0.20
U	-	0.20	0.10	0.10	0.10

Granitoid data table

Table B2						
Sample ID	G 1	G 2	G 3	G 4	G 5	G 6
TAS name	Granite	Granite	Quartz Monzonite	Granite	Granite	Quartz Monzonite
Rock Unit	Mont Orfano	Mont Orfano	Baveno Mottarone	Baveno Mottarone	Alzo Roccapietra	Alzo Roccapietra
Source	Pinarelli	Pinarelli	Pinarelli	Pinarelli	Pinarelli	Pinarelli
Method	XRF & ICPMS	XRF & ICPMS	XRF & ICPMS	XRF & ICPMS	XRF & ICPMS	XRF & ICPMS
MAJOR ELEMENTS (WT %)						
SiO_2	72.69	74.97	62.66	75.39	70.40	64.60
TiO_2	0.20	0.10	0.36	0.10	0.31	0.56
Al_2O_3	15.09	14.60	18.92	13.98	16.64	17.18
FeO^{TOT}	1.80	1.21	3.29	1.32	2.00	4.10
MnO	0.03	0.02	0.04	0.04	0.04	0.12
MgO	0.26	0.02	4.81	0.08	0.69	0.68
CaO	1.40	0.43	2.37	0.52	2.16	2.43
Na_2O	3.48	3.54	5.62	3.58	3.58	3.83
K_2O	4.78	4.97	1.45	4.81	3.84	5.88
P_2O_5	0.07	0.01	0.10	0.02	0.11	0.17
Total	99.80	99.87	99.62	99.84	99.77	99.55
TRACE ELEMENTS (PPM)						
Rb	195.00	163.00	44.00	255.00	185.00	120.00
Sr	98.00	20.00	57.00	25.00	175.00	201.00
Y	38.00	39.00	49.00	60.00	16.00	16.00
Zr	116.00	110.00	335.00	87.00	121.00	528.00
Nb	15.00	14.00	21.00	16.00	9.00	18.00
Ba	415.00	117.00	55.00	67.00	502.00	1399.00
La	44.00	38.00	116.00	29.00	22.00	219.00
Ce	91.00	81.00	234.00	68.00	43.00	390.00
Pr	-	-	-	-	-	-
Nd	43.00	37.00	97.00	38.00	19.00	140.00
Sm	9.20	8.30	16.00	10.00	3.60	15.00
Eu	0.92	0.43	1.80	0.34	1.00	2.60
Gd	8.90	8.00	12.00	11.00	3.40	9.00
Tb	-	-	-	-	-	-
Dy	8.10	7.40	8.50	12.00	3.00	3.00
Ho	-	-	-	-	-	-
Er	4.90	4.50	4.90	7.30	1.70	1.40
Tm	-	-	-	-	-	-
Yb	4.10	4.10	4.40	6.60	1.60	1.30
Lu	0.61	0.58	0.66	0.96	0.23	0.21
Hf	-	-	-	-	-	-
Ta	-	-	-	-	-	-
Th	-	-	-	-	-	-
U	-	-	-	-	-	-